View metadata, citation and similar papers at core.ac.uk

brought to you by CORE

provided by DigitalCommons@USU

Utah State University

DigitalCommons@USU

Mechanical and Aerospace Engineering Student Publications and Presentations

Mechanical and Aerospace Engineering Student Research

8-30-2019

Aerodynamic Centers of Arbitrary Airfoils Below Stall

Douglas F. Hunsaker
Utah State Univeristy, doug.hunsaker@usu.edu

Orrin D. Pope
Utah State University

Jeffrey D. Taylor
Utah State University, jeffdtaylor3891@gmail.com

Josh Hodson
Utah State University

Follow this and additional works at: https://digitalcommons.usu.edu/mae_stures

 Part of the Mechanical Engineering Commons

Recommended Citation

Hunsaker, D. F., Pope, O. D., Taylor, J. D., and Hodson, J., "Aerodynamic Centers of Arbitrary Airfoils Below Stall," Journal of Aircraft, Vol. 56, No. 6, November, 2019.

This Article is brought to you for free and open access by the Mechanical and Aerospace Engineering Student Research at DigitalCommons@USU. It has been accepted for inclusion in Mechanical and Aerospace Engineering Student Publications and Presentations by an authorized administrator of DigitalCommons@USU. For more information, please contact digitalcommons@usu.edu.

UtahStateUniversity
MERRILL-CAZIER LIBRARY

Aerodynamic Centers of Arbitrary Airfoils Below Stall

Douglas F. Hunsaker,[*] Jeffrey D. Taylor,[†] Josh Hodson,[‡] and
Utah State University, Logan, Utah 84322-4130

Orrin D. Pope[§]
Lockheed Martin Missiles and Fire Control, Grand Prairie, Texas 75051

The aerodynamic center of an airfoil is commonly estimated to lie at the quarter chord. This traditional estimate is based on thin airfoil theory, which neglects aerodynamic and geometric nonlinearities. Even below stall, these nonlinearities can have a significant effect on the location of the aerodynamic center. Here we present a method for accurately predicting the aerodynamic center of any airfoil from known lift, drag, and pitching moment data as a function of angle of attack. The method accounts for aerodynamic and geometric nonlinearities, and does not include small-angle, small-camber, and thin-airfoil approximations. It is shown that the aerodynamic center of an airfoil with arbitrary amounts of thickness and camber in an inviscid flow is a single, deterministic point, independent of angle of attack, and lies at the quarter chord only in the limit as the airfoil thickness and camber approach zero. Furthermore, it is shown that once viscous effects are included, the aerodynamic center is not a single point, but is a function of angle of attack. Differences between this general solution and that predicted by thin airfoil theory can be on the order of 3%, which is significant when predicting flutter speeds. Additionally, the results have implications for predicting the neutral point of complete aircraft.

---

[*] Assistant Professor, Mechanical and Aerospace Engineering, 4130 Old Main Hill, AIAA Senior Member.

[†] PhD Candidate, Mechanical and Aerospace Engineering, 4130 Old Main Hill, AIAA Member.

[‡] PhD Candidate, Mechanical and Aerospace Engineering, 4130 Old Main Hill, AIAA Member.

[§] Aeronautical Engineer, Aerodynamics Technology Center, AIAA Member.

Nomenclature

B_n = coefficients in the expansion given in Eq. (50)

$\tilde{\tilde{C}}_A$ = section axial-force coefficient

$\tilde{\tilde{C}}_{A,\alpha}$ = first derivative of $\tilde{\tilde{C}}_A$ with respect to α

$\tilde{\tilde{C}}_{A,\alpha,\alpha}$ = second derivative of $\tilde{\tilde{C}}_A$ with respect to α

$\tilde{\tilde{C}}_D$ = section drag coefficient

$\tilde{\tilde{C}}_{D_0}$ = section drag coefficient at zero lift

$\tilde{\tilde{C}}_{D_0,L}$ = coefficient of $\tilde{\tilde{C}}_L$ in the parabolic relation for $\tilde{\tilde{C}}_D$, Eq. (81)

$\tilde{\tilde{C}}_{D_0,L^2}$ = coefficient of $\tilde{\tilde{C}}_L^2$ in the parabolic relation for $\tilde{\tilde{C}}_D$, Eq. (81)

$\tilde{\tilde{C}}_{D_s}$ = coefficient in the relation for $\tilde{\tilde{C}}_D$ given in Eq. (96)

$\tilde{\tilde{C}}_L$ = section lift coefficient

$\tilde{\tilde{C}}_{L,\alpha}$ = first derivative of $\tilde{\tilde{C}}_L$ with respect to α

$\tilde{\tilde{C}}_{L0,\alpha}$ = first derivative of $\tilde{\tilde{C}}_L$ with respect to α, at $\alpha = 0$

$\tilde{\tilde{C}}_m$ = section moment coefficient about the point (x, y)

$\tilde{\tilde{C}}_{m_{ac}}$ = section moment coefficient about the aerodynamic center

$\tilde{\tilde{C}}_{m_{c/4}}$ = section moment coefficient about the quarter-chord

$\tilde{\tilde{C}}_{m_O}$ = section moment coefficient about the origin

$\tilde{\tilde{C}}_{m_O,\alpha}$ = first derivative of $\tilde{\tilde{C}}_{m_O}$ with respect to α

$\tilde{\tilde{C}}_{m_O,\alpha,\alpha}$ = second derivative of $\tilde{\tilde{C}}_{m_O}$ with respect to α

$\tilde{\tilde{C}}_{m,A}$ = constant coefficient used in Eqs. (58) and (83)

$\tilde{\tilde{C}}_{m,N}$ = constant coefficient used in Eqs. (58) and (83)

$\tilde{\tilde{C}}_{m0,\alpha}$ = constant coefficient used in Eqs. (58) and (83)

$\tilde{\tilde{C}}_{ms,\alpha}$ = constant coefficient used in Eqs. (62) and (99)

$\tilde{\tilde{C}}_N$ = section normal-force coefficient

$\tilde{\tilde{C}}_{N,\alpha}$ = first derivative of $\tilde{\tilde{C}}_N$ with respect to α

$\tilde{\tilde{C}}_{N,\alpha,\alpha}$ = second derivative of $\tilde{\tilde{C}}_N$ with respect to α

C_n = complex constants in the Laurent series expansion, Eq. (31)

c = section chord length

F_1, F_2 = Laurent series expansions used in Eqs. (47) and (48)

$\tilde{L}$ = section lift

$\tilde{m}_O$ = pitching moment about the origin

n = term in the Laurent series expansion

R = radius of the circular cylinder used for the conformal transformation

t = airfoil thickness

V_∞ = freestream airspeed

w = complex velocity field

w_1 = complex velocity in the plane of the circular cylinder

w_2 = complex velocity in the plane of the airfoil

x, y = axial and upward-normal coordinates relative to the leading edge

x_{ac}, y_{ac} = x and y coordinates of the aerodynamic center

y_c = y coordinate of the camber line

z = coordinate in the complex plane of the airfoil

z_l = leading edge of the airfoil in the z-plane

z_t = trailing edge of the airfoil in the z-plane

α = angle of attack

α_{L0} = zero-lift angle of attack

Γ = circulation strength

ε = thickness parameter, $\varepsilon = 0.77\,t/c$

ζ = analytic transformation function

ζ_l = point in the complex plane that maps to the airfoil leading edge

ζ_{surface} = coordinates of the cylinder surface

ζ_t = point in the complex plane that maps to the airfoil trailing edge

ζ_0 = center of the circular cylinder in the complex plane, $\zeta_0 = \xi_0 + i\eta_0$

$\kappa_{1\text{–}5}$ = constants defined in Eqs. (92) and (103)

Θ = change of variables for the axial coordinate of an airfoil

θ = angle relative to the horizontal axis in the complex plane

θ_t = value of θ at the airfoil trailing edge

ρ = fluid density

Φ_1 = complex potential in the plane of the circular cylinder

Φ_2 = complex potential in the plane of the airfoil

ξ_0 = real coordinate of the center of the circular cylinder in the complex plane

η_0 = imaginary coordinate of the center of the circular cylinder in the complex plane

I. Introduction

CORRECTLY identifying the location of the aerodynamic center of a lifting body is important in aircraft design and analysis. For example, the location of the aerodynamic center of a complete aircraft relative to the center of gravity is an important measure of static stability. The longitudinal characteristics of an aircraft are dependent on both the axial and normal distance between the aerodynamic center and the center of gravity. The aerodynamic center of a complete aircraft is often referred to as the neutral point and is a function of the aerodynamic centers of all lifting surfaces or wings comprising the aircraft. The locus of aerodynamic centers along the span of a single wing depends on the aerodynamic center of the airfoils from which the wing is constructed, as well as wing sweep, dihedral, and planform [1–3]. Furthermore, this locus of aerodynamic centers along a wing significantly impacts aeroelastic estimates for flutter and divergence speeds [4]. As Rodden points out [4], an error in the location of the aerodynamic center of only 2% can result in an 18% error relative to the elastic axis of a wing. Thus, correctly predicting the aerodynamic center or neutral point of a complete airframe during preliminary design depends on the accuracy to which the aerodynamic centers of airfoils and wings can be predicted. Here we present a method for more accurately estimating the location of the aerodynamic center of an airfoil. Although the nomenclature and development in this paper are directed toward the aerodynamics of airfoil sections, the implications of this work easily extend to allow estimates of the aerodynamic centers of finite wings and complete aircraft.

A. Traditional Relations for the Aerodynamic Center

The aerodynamic center is traditionally defined to be the point about which the pitching moment is invariant to small changes in angle of attack. For an airfoil section, this is commonly expressed as

$$\frac{\partial \tilde{C}_{m_{ac}}}{\partial \alpha} \equiv 0 \tag{1}$$

The pitching moment about any point in the airfoil plane can be found from a simple transformation of forces and moments about the origin to the point of interest, i.e.,

$$\tilde{C}_m = \tilde{C}_{m_O} + \frac{x}{c}\tilde{C}_N - \frac{y}{c}\tilde{C}_A \tag{2}$$

where $\tilde{C}_{m_O}$ is the pitching moment about the origin, $\tilde{C}_A$ is the axial force coefficient, and $\tilde{C}_N$ is the normal force coefficient. The airfoil can be located anywhere in relation to the origin of the coordinate system, but for convenience we will assume that the origin is located at the airfoil leading edge. The axial and normal force coefficients are related to the lift and drag coefficients through a transformation in angle of attack, as shown in Fig. 1

$$\tilde{C}_A = \tilde{C}_D \cos\alpha - \tilde{C}_L \sin\alpha \tag{3}$$

$$\tilde{C}_N = \tilde{C}_L \cos\alpha + \tilde{C}_D \sin\alpha \tag{4}$$

Using Eqs. (3) and (4) in Eq. (2), the pitching moment about the aerodynamic center is

$$\tilde{C}_{m_{ac}} = \tilde{C}_{m_O} + \frac{x_{ac}}{c}(\tilde{C}_L \cos\alpha + \tilde{C}_D \sin\alpha) - \frac{y_{ac}}{c}(\tilde{C}_D \cos\alpha - \tilde{C}_L \sin\alpha) \tag{5}$$

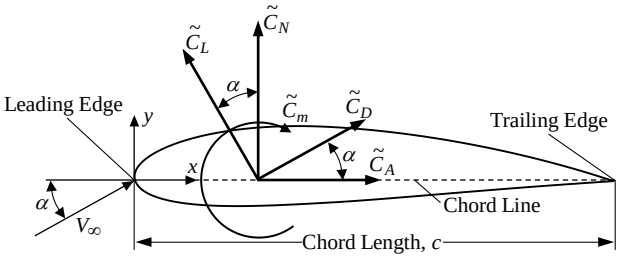

Fig. 1 Forces and pitching moment on an airfoil.

For a typical airfoil, the vertical offset of the aerodynamic center from the airfoil chord line is small, and the drag is much less than the lift. Additionally, the angle of attack is small for normal flight conditions. Therefore, applying the traditional approximations, $\tilde{C}_D \sin\alpha << \tilde{C}_L \cos\alpha$, $y_{ac} \sin\alpha << x_{ac} \cos\alpha$, $y_{ac}\tilde{C}_D << x_{ac}\tilde{C}_L$, $\cos\alpha \cong 1$, gives

$$\tilde{C}_{m_{ac}} = \tilde{C}_{m_O} + \frac{x_{ac}}{c}\tilde{C}_L \tag{6}$$

Taking the derivative of Eq. (6) with respect to angle of attack, applying the constraint given by Eq. (1), and rearranging gives the traditional approximation for the aerodynamic center

$$\frac{x_{ac}}{c} = -\frac{\tilde{C}_{m_O,\alpha}}{\tilde{C}_{L,\alpha}}, \quad \frac{y_{ac}}{c} = 0 \tag{7}$$

Note that the *y*-coordinate is traditionally assumed to be zero due to the approximations applied in the development of Eq. (6).

The relations shown in Eq. (7) are widely used today across the aerospace industry and academia. Furthermore, analogous relations have traditionally been used to approximate the location of the neutral point of complete aircraft, and are often used to evaluate aircraft static stability and compute the aircraft static margin. As will be shown, these widely used approximations suffer from several limiting assumptions and can result in errors on orders that are significant to aircraft stability and flutter analysis.

The assumptions leading to the result given in Eq. (7) include a constant lift slope and moment slope below stall, and therefore neglect any nonlinearities in lift and/or pitching moment. Additionally, any influence of drag on the aerodynamic center is entirely neglected. Furthermore, this traditional approach applies the small-angle approximation to reduce the nonlinear trigonometric relations in Eq. (5) to linear functions of angle of attack. These linearizing approximations significantly hinder our understanding of the effects of nonlinearities associated with pitch stability of airfoils and aircraft. In order to provide a more accurate solution for the location of the aerodynamic center, we shall relax the linearizing assumptions in a more general development of the aerodynamic center.

B. General Relations for the Aerodynamic Center

Phillips, Alley, and Niewoehner [3] presented general relations for the aerodynamic center, which do not include the linearizing approximations used in the traditional approach. From Eq. (2) or (5), the pitching moment about the aerodynamic center can be written

$$\tilde{C}_{m_{ac}} = \tilde{C}_{m_O} + \frac{x_{ac}}{c}\tilde{C}_N - \frac{y_{ac}}{c}\tilde{C}_A \tag{8}$$

Taking the derivative of Eq. (8) with respect to angle of attack and applying the traditional constraint given in Eq. (1) yields

$$\frac{x_{ac}}{c}\tilde{C}_{N,\alpha} - \frac{y_{ac}}{c}\tilde{C}_{A,\alpha} = -\tilde{C}_{m_O,\alpha} \tag{9}$$

Note that application of the constraint given in Eq. (1) produces an equation for a line, not a point [3,5]. The line given in Eq. (9) is the neutral axis of the airfoil [3]. All points along this line satisfy the constraint given in Eq. (1). Therefore, the single constraint given in Eq. (1) is not sufficient to specify a single point as the aerodynamic center. Phillips, Alley, and Niewoehner [3] suggest a second constraint to isolate the location of the aerodynamic center, namely, that the location of the aerodynamic center must also be invariant to small changes in angle of attack, i.e.,

$$\frac{\partial x_{ac}}{\partial \alpha} \equiv 0, \quad \frac{\partial y_{ac}}{\partial \alpha} \equiv 0 \tag{10}$$

Differentiating Eq. (9) with respect to angle of attack, and applying Eq. (10) gives

$$\frac{x_{ac}}{c}\tilde{C}_{N,\alpha,\alpha} - \frac{y_{ac}}{c}\tilde{C}_{A,\alpha,\alpha} = -\tilde{C}_{m_O,\alpha,\alpha} \tag{11}$$

The intersection of the two lines specified by Eqs. (9) and (11) defines a unique point where both of the constraints are simultaneously satisfied, and therefore defines the location of the aerodynamic center. Solving Eqs. (9) and (11) for x_{ac} and y_{ac}, and using the result in Eq. (8) gives the location of the aerodynamic center and the associated pitching moment [3]

$$\frac{x_{ac}}{c} = \frac{\tilde{C}_{A,\alpha}\tilde{C}_{m_O,\alpha,\alpha} - \tilde{C}_{m_O,\alpha}\tilde{C}_{A,\alpha,\alpha}}{\tilde{C}_{N,\alpha}\tilde{C}_{A,\alpha,\alpha} - \tilde{C}_{A,\alpha}\tilde{C}_{N,\alpha,\alpha}} \tag{12}$$

$$\frac{y_{ac}}{c} = \frac{\tilde{\tilde{C}}_{N,\alpha}\tilde{\tilde{C}}_{m_O,\alpha,\alpha} - \tilde{\tilde{C}}_{m_O,\alpha}\tilde{\tilde{C}}_{N,\alpha,\alpha}}{\tilde{\tilde{C}}_{N,\alpha}\tilde{\tilde{C}}_{A,\alpha,\alpha} - \tilde{\tilde{C}}_{A,\alpha}\tilde{\tilde{C}}_{N,\alpha,\alpha}} \tag{13}$$

$$\tilde{\tilde{C}}_{m_{ac}} = \tilde{\tilde{C}}_{m_O} + \frac{x_{ac}}{c}\tilde{\tilde{C}}_N - \frac{y_{ac}}{c}\tilde{\tilde{C}}_A \tag{14}$$

Equations (12) and (13) offer a more accurate description of the location of the aerodynamic center for any lifting body. These expressions allow both the *x* and *y* coordinates of the aerodynamic center to be evaluated, unlike the traditional approximations given in Eq. (7), which always predicts that the aerodynamic center lies on the chord line. Furthermore, Eqs. (12) and (13) correctly allow for the effects of vertical offsets, trigonometric nonlinearities, and aerodynamic nonlinearities such as drag to be included through proper treatment of the first and second aerodynamic derivatives.

If the lift, drag, and pitching moment are known from computational or experimental results at discrete angles of attack, finite differencing methods can be used to evaluate the first and second derivatives needed in Eqs. (7) or (12) and (13). However, finite differencing methods can be highly sensitive to small errors in data, especially when the data are given at small intervals in angle of attack. Most experimental data and computational results suffer from some amount of scatter, depending on how the experiment or simulation was performed. Therefore, applying finite differencing directly to such datasets can produce significant scatter in the predicted aerodynamic center of an airfoil. Hence, rather than using finite differencing methods on the data directly, these data are generally used to fit analytical expressions for lift, drag, and pitching moment as a function of angle of attack. The analytical derivatives of these expressions can then be used to obtain the required derivatives for Eqs. (12) and (13). This method for estimating derivatives reduces the impact of numerical or experimental error inherent in the data set. However, such an approach relies on an assumed form of the relationship between angle of attack, lift, drag, and pitching moment. Below stall, the lift and pitching moment are usually assumed to be linearly related to the angle of attack. This linear relationship is a result of thin airfoil theory.

C. Classical Thin Airfoil Theory

Thin airfoil theory was developed by Max Munk during the period between 1914 and 1922 [6–10], and the development of this theory can be found in many engineering text books on aerodynamics [11–16]. In this classical potential-flow theory, an airfoil is synthesized as the superposition of a uniform flow and a vortex sheet placed along

the camber line of the airfoil. Small camber and small angle-of-attack approximations are applied such that higher-order terms can be neglected. This results in the classical thin-airfoil lift and pitching-moment relations

$$\tilde{C}_L = \tilde{C}_{L,\alpha}(\alpha - \alpha_{L0}) \tag{15}$$

$$\tilde{C}_{m_O} = \tilde{C}_{m_{c/4}} - \frac{\tilde{C}_L}{4} \tag{16}$$

where $\tilde{C}_{L,\alpha}$ is the lift slope, α_{L0} is the zero-lift angle of attack, and $\tilde{C}_{m_{c/4}}$ is the pitching moment about the quarter chord. The coefficients α_{L0} and $\tilde{C}_{m_{c/4}}$ are constants that can be obtained from the camber line distribution through the relations

$$\alpha_{L0} = \frac{1}{\pi}\int_{\Theta=0}^{\pi} \frac{dy_c}{dx}(1-\cos\Theta)\,d\Theta \tag{17}$$

$$\tilde{C}_{m_{c/4}} = \frac{1}{2}\int_{\Theta=0}^{\pi} \frac{dy_c}{dx}[\cos(2\Theta)-\cos\Theta]\,d\Theta \tag{18}$$

where Θ represents the change of variables for the axial coordinate given by $x(\Theta) \equiv (c/2)(1-\cos\Theta)$. The coefficient $\tilde{C}_{L,\alpha}$ is a constant, which from thin-airfoil theory is predicted to be

$$\tilde{C}_{L,\alpha} = 2\pi \tag{19}$$

Using Eq. (15) in Eq. (16) and applying the result to the traditional relations for the aerodynamic center given in Eqs. (6) and (7) gives the aerodynamic center as predicted by thin airfoil theory,

$$\frac{x_{ac}}{c} = \frac{1}{4}, \quad \frac{y_{ac}}{c} = 0, \quad \tilde{C}_{m_{ac}} = \tilde{C}_{m_{c/4}} \tag{20}$$

Notice from Eqs. (15) and (16) that the lift and pitching moment are predicted by this theory to be linear functions of angle of attack. All higher-order terms in angle of attack were neglected in the development of these relations. Strictly speaking, Eqs. (15)–(19) are only accurate in the limit as the airfoil geometry and operating conditions approach the approximations applied in the development of classical thin airfoil theory. These assumptions include those of potential flow as well as an airfoil with zero thickness and small camber at small angles of attack. However, it is commonly assumed that the form of Eqs. (15) and (16) are correct for arbitrary airfoils at angles of attack below

stall, even with viscous effects included. Therefore, $\tilde{C}_{L,\alpha}$, α_{L0}, and $\tilde{C}_{m_{c/4}}$ are often used as coefficients to fit Eqs. (15) and (16) to airfoil data obtained from experimental measurements or numerical simulations. This results in predictions for lift and pitching moment that are linear functions of angle of attack and do not contain any higher-order dependence on angle of attack below stall.

Even with the rather constraining assumptions used in the development of thin airfoil theory, comparisons show that results from this theory are in reasonable agreement with experimental data [16]. Hence, the linear relationship between lift and angle of attack as well as pitching moment and angle of attack have been widely used. Therefore, it may appear that a reasonable estimate for the aerodynamic center of an airfoil could be obtained by applying the linear aerodynamic equations from thin airfoil theory while retaining the geometric nonlinearities of Eqs. (3) and (4). For the case of inviscid flow, i.e., $\tilde{C}_D = 0$, using Eq. (15) in Eqs. (3) and (4), differentiating the result twice along with Eq. (16), and applying the resulting derivatives to Eqs. (12)–(14) gives

$$\frac{x_{ac}}{c} = \frac{(\alpha_{L0} - \alpha)\sin\alpha + 2\cos\alpha}{4(\alpha - \alpha_{L0})^2 + 8} \tag{21}$$

$$\frac{y_{ac}}{c} = \frac{(\alpha - \alpha_{L0})\cos\alpha + 2\sin\alpha}{4(\alpha - \alpha_{L0})^2 + 8} \tag{22}$$

$$\tilde{C}_{m_{ac}} = \frac{-\tilde{C}_{L,\alpha}(\alpha - \alpha_{L0})^3 + 4\tilde{C}_{m_{c/4}}[(\alpha - \alpha_{L0})^2 + 2]}{4(\alpha - \alpha_{L0})^2 + 8} \tag{23}$$

Note that the aerodynamic center and associated pitching moment given by Eqs. (21)–(23) are nonlinear functions of angle of attack. However, because these expressions were derived using the aerodynamic coefficients from thin airfoil theory, they retain the aerodynamic linearizing assumptions. As will be shown, this approach of retaining the geometric nonlinearities given in Eqs. (3), (4), (12), and (13) while neglecting the aerodynamic nonlinearities produces a very poor approximation for the location of the aerodynamic center. From Eqs. (12) and (13), we see that the location of the aerodynamic center depends on accurately predicting any second-order aerodynamic nonlinearities, even below stall. Because thin airfoil theory neglects second-order effects, it cannot be used with Eqs. (12) and (13) to estimate second-order derivatives. Hence, some estimate for the nonlinear aerodynamic characteristics of an airfoil below stall is needed in order to accurately locate the aerodynamic center. We now consider a more general airfoil theory that retains nonlinear aerodynamic properties below stall.

II. General Inviscid Airfoil Theory

A general airfoil theory that does not include the linearizing approximations of small camber, small thickness, and small angles of attack can be developed from the method of conformal mapping [17,18], in which flow about a circular cylinder in the ζ-plane is mapped to flow about any arbitrary two-dimensional surface in the z-plane. The ζ-plane and z-plane are shown in Figs. 2 and 3. Flow about a circular cylinder of radius R centered at the point $\zeta_0 = \xi_0 + i\eta_0$, including the effects of angle of attack, α, and finite circulation, Γ, can be described in the ζ-plane by

$$w_1(\zeta) = \frac{d\Phi_1}{d\zeta} = V_\infty \left[e^{-i\alpha} + i\frac{\Gamma}{2\pi V_\infty}\frac{1}{(\zeta - \zeta_0)} - R^2 e^{i\alpha}\frac{1}{(\zeta - \zeta_0)^2} \right] \tag{24}$$

where Φ_1 is the complex potential and w_1 is the complex velocity in the plane of the circular cylinder. Using the method of conformal mapping, we can apply an arbitrary transformation of this flow from the plane of the cylinder to the plane of an airfoil of the form

$$\Phi_2(z) = \Phi_1[\zeta(z)] \tag{25}$$

where $\zeta(z)$ is an analytic transformation function. The complex velocity in the airfoil plane corresponding to this complex potential is

$$w_2(z) = \frac{d\Phi_2}{dz} = \frac{d}{d\zeta}\Phi_1[\zeta(z)]\frac{d\zeta}{dz} = w_1[\zeta(z)]\frac{d\zeta}{dz} = w_1[\zeta(z)] \Big/ \frac{dz}{d\zeta} \tag{26}$$

Thus, the complex velocity for the transformed flow field can be expressed as

$$w_2(z) = \frac{d\Phi_2}{dz} = V_\infty \left[e^{-i\alpha} + i\frac{\Gamma}{2\pi V_\infty}\frac{1}{(\zeta - \zeta_0)} - R^2 e^{i\alpha}\frac{1}{(\zeta - \zeta_0)^2} \right] \Big/ \frac{dz}{d\zeta} \tag{27}$$

The potential-flow solution about a circular cylinder can be transformed to obtain the potential-flow solution about a cylinder with any arbitrary cross section. In general, an arbitrary transformation requires an infinite number of degrees of freedom, and can be expressed in terms of the Laurent series expansion [18],

$$z(\zeta) = \zeta + \sum_{n=1}^{\infty} \frac{C_n}{\zeta^n} \tag{28}$$

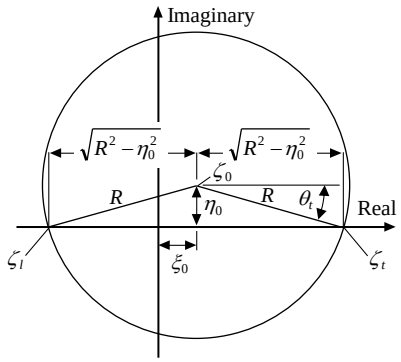

Fig. 2 Circular cylinder in the complex ζ-plane.

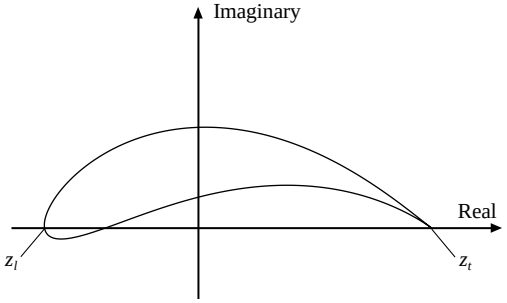

Fig. 3 Airfoil geometry in the complex *z*-plane.

where the coefficients, C_n, are complex constants. The first derivative of this general transformation is

$$\frac{dz}{d\zeta} = 1 - \sum_{n=1}^{\infty} \frac{nC_n}{\zeta^{n+1}} \tag{29}$$

The equation for the surface of the circular cylinder in the ζ-plane can be written as

$$\zeta_{\text{surface}} = R\,e^{i\theta} + \zeta_0 \tag{30}$$

Using Eq. (30) in Eq. (28), the transformed surface of the cylinder in the *z*-plane is given by the relation

$$z(\zeta_{\text{surface}}) = R\,e^{i\theta} + \zeta_0 + \sum_{n=1}^{\infty} \frac{C_n}{(R\,e^{i\theta} + \zeta_0)^n} \tag{31}$$

The derivative of the conformal transformation given in Eq. (29) can be zero at multiple points, depending on the values of the complex coefficients, C_n. These values of ζ are often referred to as the *critical points* of the transformation, at which the transformed velocity field given by Eq. (27) is singular. In order to map the flow of a

circular cylinder to that over an airfoil, one of the critical points must lie on the circular cylinder in the ζ-plane at the point that maps to the airfoil's trailing edge in the z-plane. All remaining critical points must lie inside the circular cylinder in the ζ-plane in order for the flow external to the cylinder to remain conformal. We will constrain our analysis to airfoil cross sections with only a single trailing edge at which the Kutta condition is applied. Here we denote the critical point in the ζ-plane that maps to the airfoil's trailing edge in the z-plane as ζ_t. It is convenient to choose ζ_t to be on the positive real axis, as shown in Fig. 2. This requires

$$\zeta_t = \sqrt{R^2 - \eta_0^2} + \xi_0 = R\, e^{i\theta_t} + \zeta_0 \tag{32}$$

where θ_t is the value of θ at $\zeta=\zeta_t$, i.e.,

$$\theta_t = \sin^{-1}(-\eta_0 / R) = -\tan^{-1}\left(\eta_0 \Big/ \sqrt{R^2 - \eta_0^2}\right) \tag{33}$$

Similarly, the left-hand real-axis intercept of the parent circular cylinder is

$$\zeta_l = -\sqrt{R^2 - \eta_0^2} + \xi_0 \tag{34}$$

The Kutta condition must be satisfied at the trailing edge of the airfoil, and requires that ζ_t be a stagnation point for the flow in the ζ-plane. The complex velocity field is given in Eq. (24) and will have a stagnation point at the point on the parent circular cylinder that maps to the airfoil trailing edge if

$$e^{-i\alpha} + i\frac{\Gamma}{2\pi V_\infty}\frac{1}{(\zeta_t - \zeta_0)} - R^2 e^{i\alpha}\frac{1}{(\zeta_t - \zeta_0)^2} = 0 \tag{35}$$

Solving this relation for Γ gives the circulation that will satisfy the Kutta condition at the trailing edge,

$$\Gamma = \frac{2\pi V_\infty}{i}\left[R^2 e^{i\alpha}\frac{1}{(\zeta_t - \zeta_0)} - (\zeta_t - \zeta_0)e^{-i\alpha}\right] \tag{36}$$

Using Eq. (32) we can evaluate

$$\zeta_t - \zeta_0 = \sqrt{R^2 - \eta_0^2} + \xi_0 - (\xi_0 + i\eta_0) = \sqrt{R^2 - \eta_0^2} - i\eta_0 \tag{37}$$

Using Eq. (37) in Eq. (36) gives an alternate form for the circulation

$$\Gamma = 4\pi V_\infty \left(\sqrt{R^2 - \eta_0^2} \sin\alpha + \eta_0 \cos\alpha \right) \tag{38}$$

From the Kutta-Joukowski law [19,20], the section lift can be computed from the section circulation, i.e.,

$$\tilde{L} = \rho V_\infty \Gamma \tag{39}$$

Using the circulation from Eq. (38) in Eq. (39) gives

$$\tilde{L} = 4\pi\rho V_\infty^2 \left(\sqrt{R^2 - \eta_0^2} \sin\alpha + \eta_0 \cos\alpha \right) \tag{40}$$

Notice that the predicted section lift given in Eq. (40) is independent of any particular transformation, and is a function only of the radius and vertical offset of the circular cylinder. On the other hand, the leading and trailing edges of the airfoil in the *z*-plane are dependent on the transformation, and are needed in order to compute the chord length and lift coefficient. For any given transformation, the section lift coefficient can be obtained from Eq. (40)

$$\tilde{C}_L \equiv \frac{\tilde{L}}{\frac{1}{2}\rho V_\infty{}^2 (z_t - z_l)} = \frac{8\pi\sqrt{R^2 - \eta_0^2}}{(z_t - z_l)} \left(\sin\alpha + \frac{\eta_0}{\sqrt{R^2 - \eta_0^2}} \cos\alpha \right) \tag{41}$$

where $c = z_t - z_l$ is the airfoil chord length. Thus, regardless of the transformation, the lift coefficient will be of the form

$$\tilde{C}_L = \tilde{C}_{L0,\alpha} (\sin\alpha - \tan\alpha_{L0} \cos\alpha) \tag{42}$$

where $\tilde{C}_{L0,\alpha}$ is the lift slope at zero angle of attack and α_{L0} is the zero-lift angle of attack. From Eq. (41),

$$\tilde{C}_{L0,\alpha} = \frac{8\pi\sqrt{R^2 - \eta_0^2}}{(z_t - z_l)}, \quad \alpha_{L0} = \theta_t = -\tan^{-1}\left(\eta_0 \Big/ \sqrt{R^2 - \eta_0^2} \right) \tag{43}$$

Notice that from Eqs. (40) and (43) the lift and zero-lift angle of attack do not depend on either the transformation or the real part of the cylinder offset, ξ_0. On the other hand, the lift coefficient and lift slope at zero angle of attack depend on the transformation, which in turn depends on ξ_0. In any case, **Eq. (42) is a general form for the lift coefficient of an arbitrary airfoil. No assumptions of camber, thickness, or small angle of attack were made in the**

development of Eq. (42). Therefore, we would expect this form of equation to fit the potential-flow lift properties of any arbitrary airfoil with a single trailing edge at arbitrary angles of attack.

From the Blasius relations [21,22], the pitching moment about the origin for an arbitrary geometry is

$$\tilde{m}_O = \tfrac{1}{2}\rho \,\mathrm{real}\left\{\oint_C \left[w(z)\right]^2 z\, dz\right\} \tag{44}$$

Using Eq. (29) in Eq. (27), the square of the complex velocity of the transformed flow field is

$$\left[w_2(z)\right]^2 = V_\infty^2\left[e^{-i\alpha} + i\frac{\Gamma}{2\pi V_\infty}\frac{1}{(\zeta-\zeta_0)} - R^2 e^{i\alpha}\frac{1}{(\zeta-\zeta_0)^2}\right]^2 \Bigg/ \left(1-\sum_{n=1}^{\infty}\frac{nC_n}{\zeta^{n+1}}\right)^2 \tag{45}$$

Using Eq. (45) in Eq. (44) and expanding in a Laurent series of $1/\zeta$ gives

$$\tilde{m}_O = \tfrac{1}{2}\rho V_\infty^2 \,\mathrm{real}\left\{\oint_C \left[F_1(\zeta)\right]^2 F_2(\zeta)\, d\zeta\right\} \tag{46}$$

where

$$\left[F_1(\zeta)\right]^2 = e^{-i2\alpha} + i\frac{\Gamma e^{-i\alpha}}{\pi V_\infty}\frac{1}{\zeta} + \left(i\frac{\Gamma\zeta_0 e^{-i\alpha}}{\pi V_\infty} - \frac{\Gamma^2}{4\pi^2 V_\infty^2} - 2R^2\right)\frac{1}{\zeta^2} + \cdots \tag{47}$$

$$F_2(\zeta) = \left(\zeta + \sum_{n=1}^{\infty}\frac{C_n}{\zeta^n}\right)\Bigg/\left(1-\sum_{n=1}^{\infty}\frac{nC_n}{\zeta^{n+1}}\right) = \zeta + \frac{2C_1}{\zeta} + \frac{3C_2}{\zeta^2} + \frac{4C_3 + 2C_1^{\,2}}{\zeta^3} + \cdots \tag{48}$$

and

$$\left[F_1(\zeta)\right]^2 F_2(\zeta) = e^{-i2\alpha}\zeta + i\frac{\Gamma e^{-i\alpha}}{\pi V_\infty} + \left(i\frac{\Gamma\zeta_0 e^{-i\alpha}}{\pi V_\infty} - \frac{\Gamma^2}{4\pi^2 V_\infty^2} - 2R^2 + 2C_1 e^{-i2\alpha}\right)\frac{1}{\zeta} + \cdots \tag{49}$$

Therefore, the pitching moment about the origin can be written in terms of the series

$$\tilde{m}_O = \tfrac{1}{2}\rho V_\infty^2 \,\mathrm{real}\left\{\oint_C \sum_{n=0}^{\infty}\frac{B_n}{\zeta^{n-1}} d\zeta\right\} \tag{50}$$

where

$$B_0 = e^{-i2\alpha}, \quad B_1 = i\frac{\Gamma e^{-i\alpha}}{\pi V_\infty}, \quad B_2 = i\frac{\Gamma\zeta_0 e^{-i\alpha}}{\pi V_\infty} - \frac{\Gamma^2}{4\pi^2 V_\infty^2} - 2R^2 + 2C_1 e^{-i2\alpha}, \cdots \tag{51}$$

Using Eq. (51) in Eq. (50) and integrating shows that the pitching moment is only a function of the first constant in the Laurent series,

$$\tilde{m}_O = \text{real}\left(i2\pi\rho V_\infty^2 C_1 e^{-i2\alpha} - \rho V_\infty \Gamma \zeta_0 e^{-i\alpha}\right) \tag{52}$$

After applying the Kutta-Joukowski law given in Eq. (39), the pitching moment about the origin can be written as

$$\tilde{m}_O = \text{real}\left(i2\pi\rho V_\infty^2 C_1 e^{-i2\alpha} - \tilde{L}\zeta_0 e^{-i\alpha}\right) \tag{53}$$

Using the identity $e^{i\alpha} = \cos\alpha + i\sin\alpha$ as well as the definition $\zeta_0 = \xi_0 + i\eta_0$ in Eq. (53) gives

$$\tilde{m}_O = 2\pi\rho V_\infty^2 C_1 \sin(2\alpha) - \tilde{L}\left(\xi_0 \cos\alpha + \eta_0 \sin\alpha\right) \tag{54}$$

Because the constant C_1 depends on the transformation, we see that unlike the section lift, the section pitching moment does depend on the transformation. Dividing Eq. (54) by the dynamic pressure and chord length squared, the section pitching moment coefficient relative to the origin used in the transformation can be expressed as

$$\tilde{C}_{m_O} \equiv \frac{\tilde{m}_O}{\frac{1}{2}\rho V_\infty^2 \left(z_t - z_l\right)^2} = \frac{4\pi C_1}{\left(z_t - z_l\right)^2}\sin(2\alpha) - \tilde{C}_L \frac{\xi_0 \cos\alpha + \eta_0 \sin\alpha}{z_t - z_l} \tag{55}$$

The moment coefficient about an arbitrary point in the z-plane can be found from the moment coefficient relative to the origin and the lift coefficient,

$$\tilde{C}_m = \tilde{C}_{m_O} + \tilde{C}_L \frac{x\cos\alpha + y\sin\alpha}{z_t - z_l} \tag{56}$$

Using Eq. (55) in Eq. (56) gives

$$\tilde{C}_m = \frac{4\pi C_1}{\left(z_t - z_l\right)^2}\sin(2\alpha) + \tilde{C}_L \frac{(x-\xi_0)\cos\alpha + (y-\eta_0)\sin\alpha}{z_t - z_l} \tag{57}$$

In order to compute the pitching-moment coefficient, we need to know C_1, z_t, and z_l, which must be found from the transformation. However, regardless of the transformation, the pitching-moment coefficient for an airfoil in inviscid flow about the origin of the transformation is a function of angle of attack of the form

$$\tilde{C}_{m_O} = \tilde{C}_{m0,\alpha}\sin(2\alpha) + \tilde{C}_{m,N}\tilde{C}_L \cos\alpha - \tilde{C}_{m,A}\tilde{C}_L \sin\alpha \tag{58}$$

where $\tilde{C}_{m0,\alpha}$, $\tilde{C}_{m,N}$, and $\tilde{C}_{m,A}$ are constant coefficients. Although Eq. (58) was developed using the origin of the transformation as the location about which the moment is evaluated, the form of Eq. (58) will hold for the pitching moment about any point in the domain. As can be seen from Eq. (57), the values for the coefficients $\tilde{C}_{m,N}$ and $\tilde{C}_{m,A}$ are a function of the *x* and *y* location of the pitching moment relative to the origin used in the transformation. Since the origin of the transformation has little physical meaning in the traditional airfoil coordinate system, we will define $\tilde{C}_{m,N}$ and $\tilde{C}_{m,A}$ to be the coefficients with the pitching moment evaluated at the airfoil leading edge, i.e. $x = z_l$ and $y = 0$, which is the origin of the traditional airfoil coordinate system. For any given transformation, the pitching moment of an airfoil in an inviscid flowfield evaluated at the airfoil leading edge can be found from Eq. (58) with the coefficients

$$\tilde{C}_{m0,\alpha} = \frac{4\pi C_1}{(z_t - z_l)^2}, \quad \tilde{C}_{m,N} = \frac{z_l - \xi_0}{z_t - z_l}, \quad \tilde{C}_{m,A} = \frac{\eta_0}{z_t - z_l} \tag{59}$$

The form of Eqs. (42) and (58) hold for any airfoil transformation, and therefore should accurately match the potential-flow solution for any arbitrary airfoil with a single trailing edge. These relations were developed without any approximations for airfoil thickness, camber, or angle of attack, and are not constrained under the same limitations that were used in the development of the traditional small-camber and small-angle relations given in Eqs. (15) and (16).

For the special case of a symmetric airfoil, the vertical offset of the cylinder in the ζ-plane must be zero, i.e. $\eta_0 = 0$. Using this in Eqs. (43) and (59) gives

$$\alpha_{L0} = \tilde{C}_{m,A} = 0 \tag{60}$$

Applying this result to Eq. (42) yields

$$\tilde{C}_L = \tilde{C}_{L0,\alpha} \sin\alpha \tag{61}$$

Using Eqs. (60) and (61) in Eq. (58) and applying the trigonometric identity $\sin(2\alpha) = 2\sin\alpha\cos\alpha$, we see that the pitching moment of a symmetric airfoil in inviscid flow can be written as

$$\tilde{C}_{m_O} = \tilde{C}_{ms,\alpha} \sin\alpha\cos\alpha \tag{62}$$

where

$$\tilde{C}_{ms,\alpha} = 2\tilde{C}_{m0,\alpha} + \tilde{C}_{m,N}\tilde{C}_{L0,\alpha} \tag{63}$$

Notice that the pitching moment equation given in Eq. (62) is a function of only one coefficient, $\tilde{C}_{ms,\alpha}$, instead of the three coefficients, $\tilde{C}_{m0,\alpha}$, $\tilde{C}_{m,N}$ and $\tilde{C}_{m,A}$, required to specify the pitching moment of a cambered airfoil as a function of angle of attack given in Eq. (58). Methods for estimating this coefficient as well as the required aerodynamic coefficients for arbitrary airfoil geometries are described below.

A. Determination of Aerodynamic Coefficients

Various methods can be used to generate airfoil geometries, including conformal mapping techniques, camber and thickness specification, or using splines or other curve-fitting techniques to describe the outer surface. For any airfoil geometry derived from conformal mapping, the coefficients $\tilde{C}_{L0,\alpha}$, α_{L0}, $\tilde{C}_{m0,\alpha}$, $\tilde{C}_{m,N}$, and $\tilde{C}_{m,A}$ required in Eqs. (42) and (58) can be evaluated analytically from a known parent cylinder offset and transformation by using Eqs. (43) and (59). For example, the Joukowski transformation is defined as a special case of Eq. (28) where

$$z(\zeta) = \zeta + \frac{\left(\sqrt{R^2 - \eta_0^2} + \xi_0\right)^2}{\zeta} \tag{64}$$

Using Eq. (64) as well as a given parent circular cylinder offset of ζ_0, the method described above gives the coefficients for a Joukowski airfoil

$$\begin{gathered} C_1 = \left(\sqrt{R^2 - \eta_0^2} + \xi_0\right)^2, \quad z_t = 2\left(\sqrt{R^2 - \eta_0^2} + \xi_0\right), \quad z_l = -2\frac{R^2 - \eta_0^2 + \xi_0^2}{\sqrt{R^2 - \eta_0^2} - \xi_0} \\ \tilde{C}_{L0,\alpha} = \frac{2\pi}{1 + \xi_0 \Big/ \left(\sqrt{R^2 - \eta_0^2} - \xi_0\right)}, \quad \alpha_{L0} = -\tan^{-1}\left(\eta_0 \Big/ \sqrt{R^2 - \eta_0^2}\right) \\ \tilde{C}_{m0,\alpha} = \frac{\pi}{4}\left(\frac{R^2 - \eta_0^2 - \xi_0^2}{R^2 - \eta_0^2}\right)^2, \\ \tilde{C}_{m,N} = \frac{(z_l - \xi_0)\left(\sqrt{R^2 - \eta_0^2} - \xi_0\right)}{4(R^2 - \eta_0^2)}, \quad \tilde{C}_{m,A} = \frac{\eta_0\left(\sqrt{R^2 - \eta_0^2} - \xi_0\right)}{4(R^2 - \eta_0^2)} \end{gathered} \tag{65}$$

Most airfoils in use today were not developed using conformal mapping techniques and therefore do not have an analytic transformation similar to Eq. (64) for the Joukowski airfoils. For airfoil geometries not generated from

conformal mapping techniques, the coefficients $\tilde{\tilde{C}}_{L0,\alpha}$, α_{L0}, $\tilde{\tilde{C}}_{m0,\alpha}$, $\tilde{\tilde{C}}_{m,N}$, $\tilde{\tilde{C}}_{m,A}$, and $\tilde{\tilde{C}}_{ms,\alpha}$ required for Eqs. (42) and (58) or (62) can be evaluated numerically. This can be accomplished by fitting Eqs. (42) and (58) or (62) to a set of airfoil data obtained from experimental or numerical results.

A vertical least-squares regression method for fitting aerodynamic-coefficient equations to a set of data is outlined in detail by Hunsaker et al. [23]. Given lift and pitching moment at a set of *n* angles of attack, the coefficients $\tilde{\tilde{C}}_{L,\alpha}$ and α_{L0} needed for the traditional lift equation given in Eq. (15) can be evaluated from

$$\tilde{\tilde{C}}_{L,\alpha} = \frac{\sum_{i=1}^{n} \tilde{\tilde{C}}_{L_i} \alpha_i - \alpha_{L0} \sum_{i=1}^{n} \tilde{\tilde{C}}_{L_i}}{\sum_{i=1}^{n} \alpha_i^2 - 2\alpha_{L0} \sum_{i=1}^{n} \alpha_i + n\alpha_{L0}^2} \tag{66}$$

$$\alpha_{L0} = \frac{\sum_{i=1}^{n} \tilde{\tilde{C}}_{L_i} \cdot \sum_{i=1}^{n} \alpha_i^2 - \sum_{i=1}^{n} \alpha_i \cdot \sum_{i=1}^{n} \tilde{\tilde{C}}_{L_i} \alpha_i}{\sum_{i=1}^{n} \tilde{\tilde{C}}_{L_i} \cdot \sum_{i=1}^{n} \alpha_i - n \cdot \sum_{i=1}^{n} \tilde{\tilde{C}}_{L_i} \alpha_i} \tag{67}$$

and the quarter-chord pitching moment needed for Eq. (16) can be evaluated from

$$\tilde{\tilde{C}}_{m_{c/4}} = \frac{1}{n} \sum_{i=1}^{n} \left(\tilde{\tilde{C}}_{m_{Oi}} + \frac{\tilde{\tilde{C}}_{L_i}}{4} \right) \tag{68}$$

For the special case of a symmetric airfoil, Eqs. (66)–(68) reduce to

$$a_{L0} = \tilde{\tilde{C}}_{m_{c/4}} = 0, \quad \tilde{\tilde{C}}_{L,\alpha} = \frac{\sum_{i=1}^{n} \tilde{\tilde{C}}_{L_i} \alpha_i}{\sum_{i=1}^{n} \alpha_i^2} \tag{69}$$

Similarly, this vertical least-squares regression method can be used to evaluate best-fit values for the coefficients $\tilde{\tilde{C}}_{L0,\alpha}$ and α_{L0} needed in Eq. (42), which gives

$$\alpha_{L0} = \tan^{-1} \left[\frac{\sum_{i=1}^{n} (\tilde{\tilde{C}}_{L_i} \cos\alpha_i) \cdot \sum_{i=1}^{n} \sin^2 \alpha_i - \sum_{i=1}^{n} (\tilde{\tilde{C}}_{L_i} \sin\alpha_i) \cdot \sum_{i=1}^{n} (\sin\alpha_i \cos\alpha_i)}{\sum_{i=1}^{n} (\tilde{\tilde{C}}_{L_i} \cos\alpha_i) \cdot \sum_{i=1}^{n} (\sin\alpha_i \cos\alpha_i) - \sum_{i=1}^{n} (\tilde{\tilde{C}}_{L_i} \sin\alpha_i) \cdot \sum_{i=1}^{n} \cos^2 \alpha_i} \right] \tag{70}$$

$$\tilde{C}_{L0,\alpha} = \frac{\sum_{i=1}^{n} \tilde{C}_{L_i} (\sin\alpha_i - \tan\alpha_{L0} \cos\alpha_i)}{\sum_{i=1}^{n} (\sin\alpha_i - \tan\alpha_{L0} \cos\alpha_i)^2} \tag{71}$$

For the moment coefficients needed in Eq. (58), the vertical least-squares-regression method gives

$$\begin{Bmatrix} \tilde{C}_{m0,\alpha} \\ \tilde{C}_{m,N} \\ \tilde{C}_{m,A} \end{Bmatrix} = \begin{bmatrix} \sum_{i=1}^{n} \sin^2(2\alpha_i) & \sum_{i=1}^{n} \tilde{C}_{L_i} \cos\alpha_i \sin(2\alpha_i) & -\sum_{i=1}^{n} \tilde{C}_{L_i} \sin\alpha_i \sin(2\alpha_i) \\ \sum_{i=1}^{n} \tilde{C}_{L_i} \cos\alpha_i \sin(2\alpha_i) & \sum_{i=1}^{n} \tilde{C}_{L_i}{}^2 \cos^2\alpha_i & -\sum_{i=1}^{n} \tilde{C}_{L_i}{}^2 \cos\alpha_i \sin\alpha_i \\ \sum_{i=1}^{n} \tilde{C}_{L_i} \sin\alpha_i \sin(2\alpha_i) & \sum_{i=1}^{n} \tilde{C}_{L_i}{}^2 \cos\alpha_i \sin\alpha_i & -\sum_{i=1}^{n} \tilde{C}_{L_i}{}^2 \sin^2\alpha_i \end{bmatrix}^{-1} \begin{Bmatrix} \sum_{i=1}^{n} \tilde{C}_{m_{Oi}} \sin(2\alpha_i) \\ \sum_{i=1}^{n} \tilde{C}_{m_{Oi}} \tilde{C}_{L_i} \cos\alpha_i \\ \sum_{i=1}^{n} \tilde{C}_{m_{Oi}} \tilde{C}_{L_i} \sin\alpha_i \end{Bmatrix} \tag{72}$$

For symmetric airfoils, Eqs. (70) and (71) reduce to

$$\alpha_{L0} = 0, \quad \tilde{C}_{L0,\alpha} = \frac{\sum_{i=1}^{n} \tilde{C}_{L_i} \sin\alpha_i}{\sum_{i=1}^{n} \sin^2\alpha_i} \tag{73}$$

and the pitching-moment coefficient, $\tilde{C}_{ms,\alpha}$, required for Eq. (62) can be obtained from

$$\tilde{C}_{ms,\alpha} = \frac{\sum_{i=1}^{n} \tilde{C}_{m_{Oi}} \sin\alpha_i \cos\alpha_i}{\sum_{i=1}^{n} (\sin\alpha_i \cos\alpha_i)^2} \tag{74}$$

Equations (66)–(74) can be used to obtain the corresponding aerodynamic coefficients for any arbitrary airfoil geometry. To demonstrate how this is done, we now consider sample results for airfoils from the NACA 4-digit series.

B. Comparison to Inviscid Computational Results

Because the general airfoil theory relations given in Eqs. (42) and (58) were developed without any assumptions for airfoil geometry other than that of a single trailing edge, we should expect the form of these equations to match inviscid airfoil aerodynamic data more accurately than Eqs. (15) and (16), which were obtained from thin airfoil theory. Here we consider the accuracy of each of these equations for the NACA 4-digit series over a range of camber and thickness.

Inviscid incompressible aerodynamic lift- and pitching-moment-coefficient data for 150 NACA 4-digit series airfoils were generated over a wide range of camber and thickness using a numerical vortex panel method employing linear vortex sheets along the airfoil surface [24]. The airfoil surfaces were discretized using 400 panels, which produced grid-resolved solutions. The panels were clustered near the leading and trailing edges of the airfoil using standard cosine clustering. All computations were performed using double-precision computation. Results were computed for each airfoil at angles of attack ranging from –15 to +15 degrees in increments of 1 degree. At each angle of attack, the lift and pitching-moment coefficient about the airfoil leading edge were recorded.

The least-squares regression method given in Eqs. (66)–(69) was used to fit the aerodynamic data for each airfoil to the thin-airfoil-theory equations given in Eqs. (15) and (16), and the root-mean-square (RMS) value for each case was recorded. Similarly, the least-squares regression method given in Eqs. (70)–(74) was used to fit the aerodynamic data for each airfoil to the general airfoil theory equations given in Eqs. (42) and (58) or (62), and the RMS value for each case was recorded. Table 1 shows sample resulting coefficients for the NACA 2412 airfoil, along with the associated RMS error from both thin airfoil theory and general airfoil theory.

Table 1. Coefficients for a NACA 2412 airfoil evaluated by fitting results from the vortex panel method to relations from thin airfoil theory and general airfoil theory. RMS error are included for each fit.

Coefficient	Thin Airfoil Theory	Coefficient	General Airfoil Theory
$\tilde{C}_{L,\alpha}$	6.87991	$\tilde{C}_{L0,\alpha}$	6.93038
α_{L0}	-0.03748	α_{L0}	-0.03765
$\tilde{C}_{m_{c/4}}$	-0.05580	$\tilde{C}_{m0,\alpha}$	0.70133
		$\tilde{C}_{m,N}$	-0.46413
		$\tilde{C}_{m,A}$	0.01214

RMS Error	Thin Airfoil Theory	General Airfoil Theory
$\tilde{C}_L$	0.00444	machine zero
$\tilde{C}_m$	0.00746	machine zero

Note that the RMS error from thin airfoil theory is on the order of 0.005 while the RMS error from general airfoil theory is on the order of machine precision. These results were typical for the 150 airfoils tested with an average RMS of thin airfoil theory of 0.0119 and all results matching the general airfoil theory to machine precision. This indicates

that the general airfoil theory equations can be fit exactly to the inviscid solutions, and therefore, are of the correct form. The error associated with the least-squares regression fits to the thin airfoil theory equations indicate that the form of the thin airfoil theory equations are not exactly correct. With current measurement technology for experimental setups, the accuracy gained from the general airfoil theory equations for lift and pitching moment predictions is clearly unwarranted. Experimental data is generally known to only 2 or 3 significant figures, which is the same order of accuracy as that obtained from thin airfoil theory. **Therefore, the significance of the general airfoil theory is not that it can more accurately fit experimental data or computational results.** Indeed, the error in experimental data or CFD simulations often falls outside the range of accuracy to be found in either the general airfoil theory or thin airfoil theory. Thus, using one theory over the other will not give significantly improved results if we wish only to predict lift or pitching moment over a range of angles of attack below stall. **Rather, the significance of the general airfoil theory becomes apparent when second derivatives for lift or pitching moment as a function of angle of attack are needed.** Such is the case in the estimation of the location of the aerodynamic center.

III. The Aerodynamic Center of Airfoils in Inviscid Flow

In general, the location of the aerodynamic center can be correctly predicted using Eqs. (12) and (13). Recall that this definition for the location of the aerodynamic center is a general definition, in that it does not include any linearizing or small-angle approximations. We shall now consider the location of the aerodynamic center of inviscid airfoils as predicted by the relations developed from general airfoil theory compared with the relations developed from classical thin airfoil theory. First we consider only the case of inviscid flow, i.e., $\tilde{C}_D = 0$. From Eqs. (3) and (4), this gives

$$\tilde{C}_A = -\tilde{C}_L \sin\alpha \tag{75}$$

$$\tilde{C}_N = \tilde{C}_L \cos\alpha \tag{76}$$

The aerodynamic center of an arbitrary inviscid airfoil can be found by using the lift and pitching-moment relations from general airfoil theory. Using Eqs. (42) and (58) in Eqs. (75) and (76), differentiating twice, and applying the resulting derivatives to Eqs. (12)–(14) gives

$$\frac{x_{ac}}{c} = -2\frac{\tilde{C}_{m0,\alpha}}{\tilde{C}_{L0,\alpha}}\cos^2\alpha_{L0} - \tilde{C}_{m,N} \tag{77}$$

$$\frac{y_{ac}}{c} = \frac{\tilde{C}_{m0,\alpha}}{\tilde{C}_{L0,\alpha}}\sin(2\alpha_{L0}) + \tilde{C}_{m,A} \tag{78}$$

$$\tilde{C}_{m_{ac}} = \tilde{C}_{m0,\alpha}\sin(2\alpha_{L0}) \tag{79}$$

For the special case of a symmetric airfoil, using Eqs. (61) and (62) in the same process yields

$$\frac{x_{ac}}{c} = -\frac{\tilde{C}_{ms,\alpha}}{\tilde{C}_{L0,\alpha}}, \quad \frac{y_{ac}}{c} = 0, \quad \tilde{C}_{m_{ac}} = 0 \tag{80}$$

Notice that Eqs. (77)–(80) are independent of angle of attack. **Therefore, the location of the aerodynamic center for an arbitrary airfoil in inviscid flow is a single point, independent of angle of attack.** This same conclusion was arrived at by Karamcheti [18], who also used conformal mapping to demonstrate that "there is a point about which the moment remains unaltered as the angle of attack is varied." This point does not in general lie on the chord line at the airfoil quarter chord, but is a single deterministic point dependent on airfoil thickness and camber. This solution was developed from general airfoil theory, which does not make any assumptions for small angles of attack, small camber, or small thickness. It is rather remarkable that when all geometric and aerodynamic nonlinearities are retained in the lift and pitching moment equations, along with those in the definition of the aerodynamic center, the relations for the aerodynamic center reduce to such a simple expression, independent of angle of attack, for inviscid flow.

Figure 4 shows the aerodynamic center for the NACA 2412 airfoil as predicted by the traditional expressions given in Eqs. (7) and (20), thin airfoil theory with trigonometric nonlinearities given in Eqs. (21) and (22), and the general airfoil theory given in Eqs. (77) and (78). Figure 5 shows the corresponding pitching moment about the aerodynamic center predicted by each theory as a function of angle of attack. Note that the aerodynamic center predicted by Eqs. (77) and (78) does not lie at the quarter-chord, but is a single point 1.20% chord aft and 0.45% chord above the quarter-chord point. The pitching moment at the quarter chord shown in Table 1 deviates from the pitching moment about the aerodynamic center predicted from general airfoil theory by about 5.77%. Equations (21)–(23) represent a mix of using linear aerodynamics from thin airfoil theory while retaining the trigonometric nonlinearities

given in Eqs. (75) and (76). This produces non-physical results and should never be used to approximate the aerodynamic center and associated pitching moment.

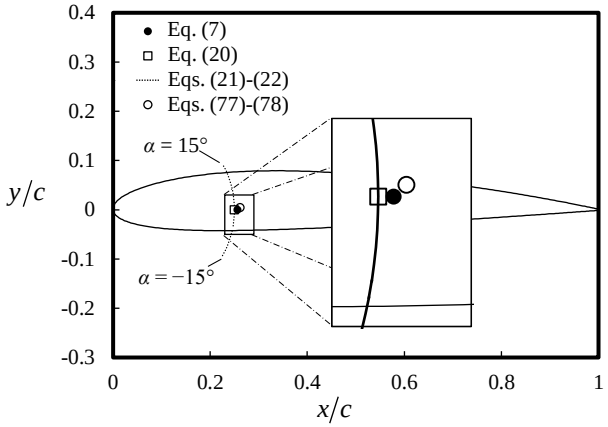

Fig. 4 The location of the aerodynamic center for a NACA 2412 airfoil in inviscid flow as predicted by traditional theories and the general airfoil theory.

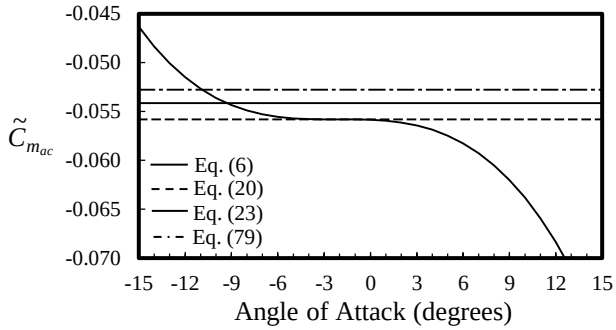

Fig. 5 Pitching moment about the aerodynamic center for the NACA 2412 airfoil in inviscid flow as predicted by traditional theories and the general airfoil theory.

To understand how thickness and camber affect the location of the aerodynamic center, the aerodynamic center as predicted from Eqs. (77) and (78) or (80) was computed for 150 NACA 4-digit-series airfoils as a function of camber and thickness. These results are shown in Fig. 6, and the corresponding predictions for the pitching moment at the aerodynamic center are shown in Fig. 7. Note that increasing thickness tends to shift the aerodynamic center aft, while camber tends to shift the aerodynamic center normal to the chord line. The aft movement of the aerodynamic center with increasing thickness was also predicted by Alan Pope [25]. Pope calculated the axial deviation of the

aerodynamic center from the quarter chord due to thickness based on an improved lift slope estimated from conformal mapping of Joukowski airfoils. His approximation can be written as

$$\frac{x_{ac}}{c} = \frac{1}{2} - \frac{1}{4(1+\varepsilon^2)(1+\varepsilon)}$$

where $\varepsilon = 0.77\,t/c$ and t/c is the percent thickness. His solution predicts an axial deviation as a function of thickness "being at the 26.7 per cent point of an airfoil 9 per cent thick and at the 27.6 per cent point for one 15 per cent thick" [25], but neglects any vertical deviation. Note that the axial deviations shown in Fig. 6 for the 4-digit NACA airfoils are smaller than those predicted by Pope [25], which were based on Joukowski airfoils [26]. Hence, the deviation of the aerodynamic center due to airfoil thickness depends on the family of airfoils considered.

Because the static margin is often on the order of 5% for a stable aircraft, the difference in the approximations for the location of the aerodynamic center obtained from general airfoil theory compared to the traditional approximations can be significant. Furthermore, because flutter analysis is highly dependent on the distance between the locus of aerodynamic centers and the elastic or torsional axis of the wing, correctly identifying the locus of aerodynamic centers along a wing can be critical. We have thus far considered only the case of inviscid flow. As will be shown, viscosity also significantly impacts the location of the aerodynamic center of an airfoil.

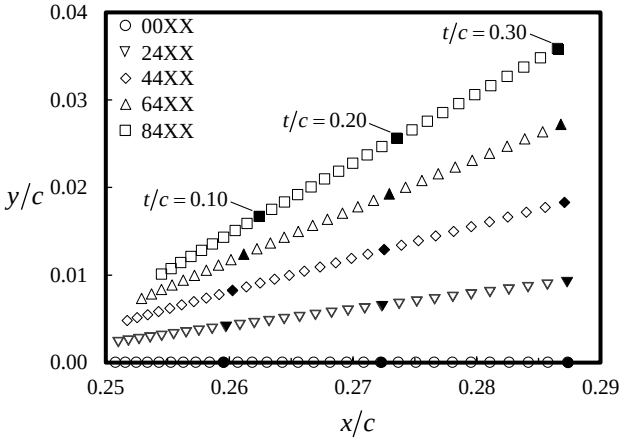

Fig. 6 The aerodynamic center location predicted from Eqs. (77) and (78) or (80) for 150 NACA 4-digit airfoils as a function of camber and thickness. Filled markers represent airfoil thickness increments of 10%.

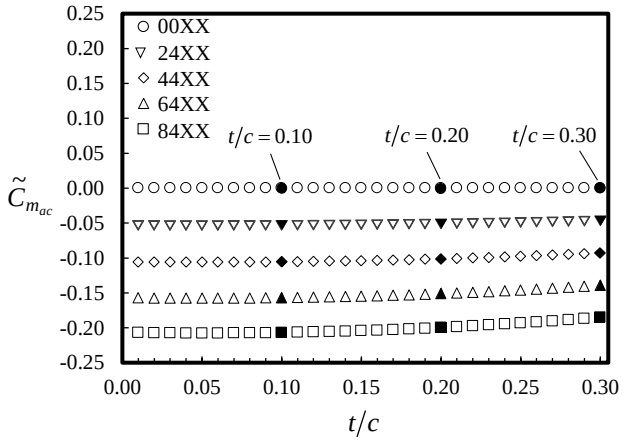

Fig. 7 Pitching moment about the aerodynamic center predicted from Eqs. (79) or (80) for 150 NACA 4-digit airfoils as a function of camber and thickness.

IV. Viscous Effects

In the previous two sections we neglected the influence of viscosity on the aerodynamic forces and moments created by an airfoil. The largest effect of viscosity on airfoils at angles of attack below stall is the production of friction along the surface of the airfoil. Below stall, this skin friction generally does not significantly impact the lift but does produce drag and alters the pitching moment relative to the inviscid scenario. The section drag coefficient is traditionally related to the section lift coefficient using a quadratic equation. Here we use the traditional relation

$$\tilde{C}_D = \tilde{C}_{D_0} + \tilde{C}_{D_0,L}\tilde{C}_L + \tilde{C}_{D_0,L^2}\tilde{C}_L^2 \tag{81}$$

where $\tilde{C}_{D_0}$, $\tilde{C}_{D_0,L}$, and $\tilde{C}_{D_0,L^2}$ are constant coefficients for a given airfoil drag polar. Note that the second term on the right-hand side is required to adequately describe drag polars that do not have a minimum at zero lift. Such is the case for most non-symmetric airfoils.

Viscosity also affects the pitching moment produced by the airfoil. Recall that Eq. (58) was developed from airfoil theory based on conformal mapping, which is built on the assumption of an inviscid flow. This equation for the pitching moment can be extended to account for viscous effects by including the drag-component acting in the normal and axial directions,

$$\tilde{C}_{m_O} = \tilde{C}_{m0,\alpha}\sin(2\alpha) + \tilde{C}_{m,N}\tilde{C}_N + \tilde{C}_{m,A}\tilde{C}_A \tag{82}$$

or, in light of Eqs. (3) and (4),

$$\tilde{C}_{m_O} = \tilde{C}_{m0,\alpha}\sin(2\alpha) + \tilde{C}_{m,N}(\tilde{C}_L\cos\alpha + \tilde{C}_D\sin\alpha) + \tilde{C}_{m,A}(\tilde{C}_D\cos\alpha - \tilde{C}_L\sin\alpha) \tag{83}$$

Differentiating Eq. (82) with respect to angle of attack and applying the result to Eqs. (12) and (13) gives the exact solution for the location of the aerodynamic center including viscous effects

$$\frac{x_{ac}}{c} = -2\tilde{C}_{m0,\alpha}\frac{2\sin(2\alpha)\tilde{C}_{A,\alpha} + \cos(2\alpha)\tilde{C}_{A,\alpha,\alpha}}{\tilde{C}_{N,\alpha}\tilde{C}_{A,\alpha,\alpha} - \tilde{C}_{A,\alpha}\tilde{C}_{N,\alpha,\alpha}} - \tilde{C}_{m,N} \tag{84}$$

$$\frac{y_{ac}}{c} = -2\tilde{C}_{m0,\alpha}\frac{2\sin(2\alpha)\tilde{C}_{N,\alpha} + \cos(2\alpha)\tilde{C}_{N,\alpha,\alpha}}{\tilde{C}_{N,\alpha}\tilde{C}_{A,\alpha,\alpha} - \tilde{C}_{A,\alpha}\tilde{C}_{N,\alpha,\alpha}} + \tilde{C}_{m,A} \tag{85}$$

Applying Eqs. (82), (84), and (85) to Eq. (14) gives the associated pitching moment

$$\tilde{C}_{m_{ac}} = \tilde{C}_{m0,\alpha}\left[\sin(2\alpha) + 2\frac{2\sin(2\alpha)(\tilde{C}_{N,\alpha}\tilde{C}_A - \tilde{C}_N\tilde{C}_{A,\alpha}) + \cos(2\alpha)(\tilde{C}_A\tilde{C}_{N,\alpha,\alpha} - \tilde{C}_N\tilde{C}_{A,\alpha,\alpha})}{\tilde{C}_{N,\alpha}\tilde{C}_{A,\alpha,\alpha} - \tilde{C}_{A,\alpha}\tilde{C}_{N,\alpha,\alpha}}\right] \tag{86}$$

In order to complete the formulation, first and second derivatives for the axial- and normal-force coefficients needed in Eqs. (84)–(86) must be obtained. Expressions for these derivatives with respect to angle of attack can be found analytically by using Eqs. (42) and (81) in Eqs. (3) and (4) and differentiating. The process for obtaining each of these derivatives is rather straight forward and can be performed by a symbolic solver. The details will not be included here. Once obtained, these derivatives can be used in Eqs. (84), (85), and (86) to find the exact location of the aerodynamic center and associated pitching moment including viscous effects. The result is a rather lengthy set of equations. However, as can be seen from Eqs. (84) and (85), **the location of the aerodynamic center of an arbitrary airfoil including the effects of viscosity is a function of angle of attack.** This differs from the inviscid solution given in Eqs. (77) and (78), which yield a single point independent of angle of attack.

The first and second derivatives of the axial- and normal-force coefficients required for Eqs. (84)–(86) are quite cumbersome to use in practice, although they can be very useful if applied in a computational framework. A simplified approximation for the location of the aerodynamic center can be obtained by applying the third-order small-angle approximations

$$\begin{gathered}\sin\alpha \cong \alpha - \alpha^3/6, \quad \sin(2\alpha) \cong 2\alpha - 4\alpha^3/3, \quad \sin(3\alpha) \cong 3\alpha - 9\alpha^3/2, \\ \cos\alpha \cong 1 - \alpha^2/2, \quad \cos(2\alpha) \cong 1 - 2\alpha^2, \\ \cos(3\alpha) \cong 1 - 9\alpha^2/2, \quad \tan\alpha_{L0} \cong \alpha_{L0} + \alpha_{L0}^3/3\end{gathered} \tag{87}$$

to Eqs. (84)–(86) as well as to the first and second derivatives of the axial- and normal-force coefficients required in these equations. Because the angle of attack α, zero-lift angle of attack α_{L0}, and drag are small compared to the section lift slope $\tilde{C}_{L0,\alpha}$, we neglect any terms that include fourth-order and higher combinations of α, α_{L0}, $\tilde{C}_{D_0}$, $\tilde{C}_{D_0,L}$, and $\tilde{C}_{D_0,L^2}$. For airfoils at angles of attack below stall, values for these coefficients generally fall in the ranges $-0.2 < \alpha < 0.3$, $-0.1 < \alpha_{L0} < 0.1$, $0.004 < \tilde{C}_{D_0} < 0.010$, $-0.003 < \tilde{C}_{D_0,L} < 0$, $0.003 < \tilde{C}_{D_0,L^2} < 0.015$. Therefore, we also apply the following simplifying approximations

$$\begin{gathered}\tilde{C}_{D_0,L}\alpha_{L0} << 1, \quad \tilde{C}_{D_0,L}\alpha << 1, \\ \tilde{C}_{D_0}\tilde{C}_{D_0,L^2} << 1, \quad \tilde{C}_{D_0}^2 << 1, \quad \tilde{C}_{D_0,L}^2 << 1\end{gathered} \tag{88}$$

This process produces what will be referred to here as the third-order approximation for the aerodynamic center and associated pitching moment, which can be written as

$$\frac{x_{ac}}{c} = -2\frac{\tilde{C}_{m0,\alpha}}{\tilde{C}_{L0,\alpha}}\left[\frac{\kappa_1[3(\alpha\alpha_{L0} - \alpha^2 - \alpha_{L0}^2/2) + 1] - \kappa_2(1 + 3\alpha^2/2) - 1}{\kappa_1(1 + 3\alpha_{L0}^2/2) + 3\kappa_2(\alpha^2/2 - \alpha\alpha_{L0} - 2\kappa_2/3 - 1) - \alpha_{L0}^2 - 1}\right] - \tilde{C}_{m,N} \tag{89}$$

$$\frac{y_{ac}}{c} = -2\frac{\tilde{C}_{m0,\alpha}}{\tilde{C}_{L0,\alpha}}\left[\frac{\kappa_1(3\alpha - 2\alpha_{L0}) + \tilde{C}_{D_0,L} + 3\alpha\kappa_2 + \alpha_{L0}(1 + \alpha_{L0}^2/3)}{\kappa_1(1 + 3\alpha_{L0}^2/2) + 3\kappa_2(\alpha^2/2 - \alpha\alpha_{L0} - 2\kappa_2/3 - 1) - \alpha_{L0}^2 - 1}\right] + \tilde{C}_{m,A} \tag{90}$$

$$\tilde{C}_{m_{ac}} = 2\tilde{C}_{m0,\alpha}\left[\frac{\alpha_{L0}(\kappa_1 + \kappa_2 - \alpha_{L0}^2/3 - 1) + 6\alpha\kappa_2(\kappa_1 + \kappa_2)}{\kappa_1(1 + 3\alpha_{L0}^2/2) + 3\kappa_2(\alpha^2/2 - \alpha\alpha_{L0} - 2\kappa_2/3 - 1) - \alpha_{L0}^2 - 1}\right] \tag{91}$$

where

$$\kappa_1 \equiv \tilde{C}_{L0,\alpha}\tilde{C}_{D_0,L^2}, \quad \kappa_2 \equiv \tilde{C}_{D_0}/(2\tilde{C}_{L0,\alpha}) \tag{92}$$

Equations (89)–(92) can be used as an accurate estimate for the aerodynamic center and associated pitching moment for any cambered airfoil below stall. Of course, the accuracy of any estimate for the aerodynamic center is also dependent on the accuracy to which the coefficients in Eqs. (42), (81), and (83) are known.

The aerodynamic coefficients required for Eqs. (89)–(92) including viscous effects can be obtained from a set of data using the least-squares regression method outlined by Hunsaker et al. [23]. Because viscosity produces only a small effect on lift, the least-squares solution given in Eqs. (70) and (71) can be used to obtain the aerodynamic coefficients needed to predict lift as a function of angle of attack given in Eq. (42). The aerodynamic coefficients needed for the drag polar equation given in Eq. (81) can be obtained from

$$\begin{Bmatrix} \tilde{C}_{D_0} \\ \tilde{C}_{D_0,L} \\ \tilde{C}_{D_0,L^2} \end{Bmatrix} = \begin{bmatrix} n & \sum_{i=1}^{n} \tilde{C}_{L_i} & \sum_{i=1}^{n} \tilde{C}_{L_i}^{\,2} \\ \sum_{i=1}^{n} \tilde{C}_{L_i} & \sum_{i=1}^{n} \tilde{C}_{L_i}^{\,2} & \sum_{i=1}^{n} \tilde{C}_{L_i}^{\,3} \\ \sum_{i=1}^{n} \tilde{C}_{L_i}^{\,2} & \sum_{i=1}^{n} \tilde{C}_{L_i}^{\,3} & \sum_{i=1}^{n} \tilde{C}_{L_i}^{\,4} \end{bmatrix}^{-1} \begin{Bmatrix} \sum_{i=1}^{n} \tilde{C}_{D_i} \\ \sum_{i=1}^{n} \tilde{C}_{D_i} \tilde{C}_{L_i} \\ \sum_{i=1}^{n} \tilde{C}_{D_i} \tilde{C}_{L_i}^{\,2} \end{Bmatrix} \tag{93}$$

In a similar manner, the aerodynamic coefficients needed for the pitching-moment equation given in Eq. (83) can be obtained from

$$\begin{Bmatrix} \tilde{C}_{m0,\alpha} \\ \tilde{C}_{m,N} \\ \tilde{C}_{m,A} \end{Bmatrix} = \begin{bmatrix} \sum_{i=1}^{n} \sin^2(2\alpha_i) & \sum_{i=1}^{n} \sin(2\alpha_i) \tilde{C}_{N_i} & \sum_{i=1}^{n} \sin(2\alpha_i) \tilde{C}_{A_i} \\ \sum_{i=1}^{n} \sin(2\alpha_i) \tilde{C}_{N_i} & \sum_{i=1}^{n} \tilde{C}_{N_i}^{\,2} & \sum_{i=1}^{n} \tilde{C}_{N_i} \tilde{C}_{A_i} \\ \sum_{i=1}^{n} \sin(2\alpha_i) \tilde{C}_{A_i} & \sum_{i=1}^{n} \tilde{C}_{N_i} \tilde{C}_{A_i} & \sum_{i=1}^{n} \tilde{C}_{A_i}^{\,2} \end{bmatrix}^{-1} \begin{Bmatrix} \sum_{i=1}^{n} \tilde{C}_{m_{Oi}} \sin(2\alpha_i) \\ \sum_{i=1}^{n} \tilde{C}_{m_{Oi}} \tilde{C}_{N_i} \\ \sum_{i=1}^{n} \tilde{C}_{m_{Oi}} \tilde{C}_{A_i} \end{Bmatrix} \tag{94}$$

where $\tilde{C}_{Ai} = \tilde{C}_{D_i} \cos\alpha_i - \tilde{C}_{L_i} \sin\alpha_i$ and $\tilde{C}_{Ni} = \tilde{C}_{L_i} \cos\alpha_i + \tilde{C}_{D_i} \sin\alpha_i$.

A. Example Results

Data for several NACA 4-digit airfoils at a Reynolds number near 3.0E06 were digitized from plots of lift, drag, and pitching moment published by Abbott and von Doenhoff [27]. These data were fit to Eqs. (42), (81), and (83) using the least-squares regression equations given in Eqs. (70), (71), (93), and (94). The resulting aerodynamic coefficients for these airfoils are shown in Table 2. Figure 8 shows the aerodynamic center location for each of these airfoils over the range $-15 \le \alpha \le 15$ as computed from the exact solution obtained from analytical derivatives applied to Eqs. (84) and (85), as well as the third-order estimate from Eqs. (89) and (90). As can be seen from these results,

Eqs. (89) and (90) quite accurately match the exact solutions for each of the airfoils considered. Note that at positive angles of attack, the aerodynamic center is positioned higher than at negative angles of attack. This vertical deviation can be as large as 2% of the chord. Also notice that the aerodynamic center predictions including viscous effects deviate from the quarter chord by as much as 3.5% in the axial direction and 4.5% in the normal direction as a percentage of chord for this set of airfoils. While the deviation of the aerodynamic center from the commonly used approximation of the quarter chord may seem insignificant, these magnitudes can be significant for flutter estimates. Additionally, results have strong implications for the pitch stability of complete aircraft, which generally have a static margin on the order of 5% of the main wing mean chord. For most aircraft, accurately estimating the axial location of the aerodynamic center is usually more important than accurately estimating the vertical location of the aerodynamic center. This is because the vertical offset between the center of gravity and the aerodynamic center is small for most aircraft. However, as pointed out by Phillips, Alley, and Niewoehner [3], "if the center of gravity of an airplane is substantially above or below the aerodynamic center, nonlinear effects can have a detrimental effect on pitch stability by producing large variations in the pitch-stability derivative with angle of attack." This can be the case for high-wing aircraft and hang gliders.

Table 2. Coefficients for several NACA airfoils as computed from the vertical least-squares algorithm using data from Abbott and von Doenhoff [27].

NACA	α_{L0}	$\tilde{\tilde{C}}_{L0,\alpha}$	$\tilde{\tilde{C}}_{D_0}$	$\tilde{\tilde{C}}_{D_0,L}$	$\tilde{\tilde{C}}_{D_0,L^2}$	$\tilde{\tilde{C}}_{m0,\alpha}$	$\tilde{\tilde{C}}_{m,A}$	$\tilde{\tilde{C}}_{m,N}$
1408	-0.01457	6.18977	0.00515	-0.00176	0.00802	0.86774	-0.03221	-0.53493
1412	-0.02160	6.02468	0.00587	-0.00135	0. 00537	0. 54239	-0. 01838	-0. 42972
2412	-0.04556	5.75810	0.00640	-0.00208	0.00619	0.49412	-0.02634	-0.41442
2424	-0.03540	5.18830	0.00845	-0.00076	0.00636	0.56386	0.02839	-0.43311
4415	-0.07343	5.68654	0.00751	-0.00254	0.00419	0.64057	-0.02452	-0.46852
4418	-0.06851	5.71103	0.00790	-0.00256	0.00401	0.66330	-0.02351	-0.47075
4424	-0.06285	5.38038	0.00879	-0.00178	0.00533	0.68051	-0.00591	-0.47971

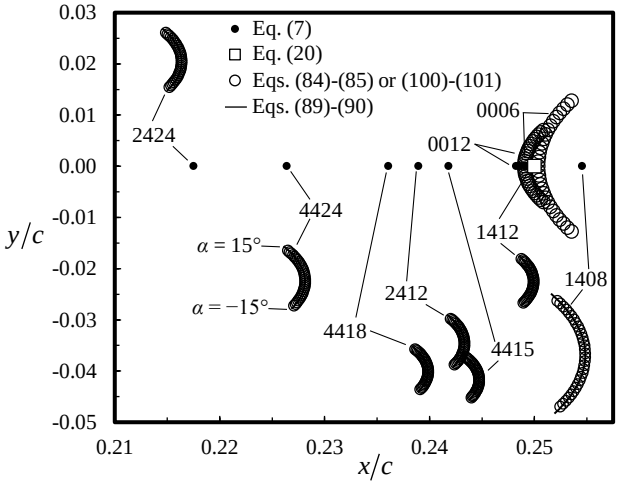

Fig. 8 Predicted aerodynamic centers of several NACA 4-digit airfoils including viscous effects at a Reynolds number of 3.0E6 over the range $-15 \leq \alpha \leq 15$.

To understand how large the deviation of the aerodynamic center as a function of angle of attack can be in comparison to the airfoil geometry, results for the NACA 2412 airfoil are shown in Fig. 9. Predictions for the aerodynamic center from four methods are included. These include the traditional solutions from Eqs. (7) and (20), the inviscid solution from Eqs. (77) and (78) using data from the panel method [24], and the full viscous solution from Eqs. (84) and (85) using data from Abbott and von Doenhoff [27]. Also included is the estimate given in Eqs. (89) and (90), which nearly identically overlap the exact solution from Eqs. (84) and (85). Note that while the traditional solutions given in Eqs. (7) and (20) and the inviscid solution given in Eqs. (77) and (78) predict an aerodynamic center that is independent of angle of attack, the full viscous solution predicts that the aerodynamic center is a function of angle of attack.

Figure 10 shows the pitching moment for the NACA 2412 airfoil as a function of angle of attack predicted from the traditional method as well as the methods suggested in this paper. In this case, thin airfoil theory matches the full viscous solution surprisingly well, partially due to the fact that viscosity tends to cancel thickness effects [24].

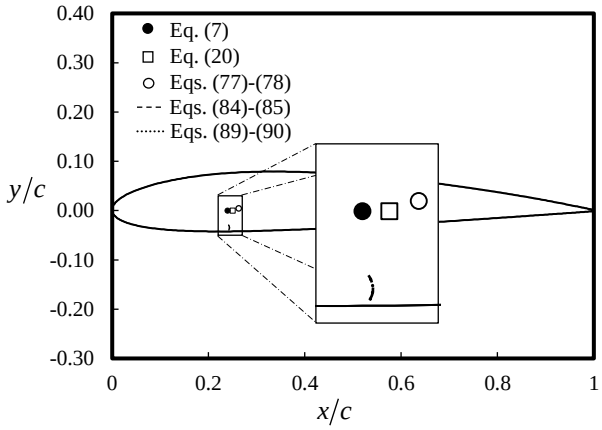

Fig. 9 Aerodynamic center locations for the NACA 2412 airfoil as predicted by traditional methods compared to the methods presented in this paper. Note that the location predicted by Eqs. (84)-(85) lies directly on top of that predicted by Eqs. (89)-(90).

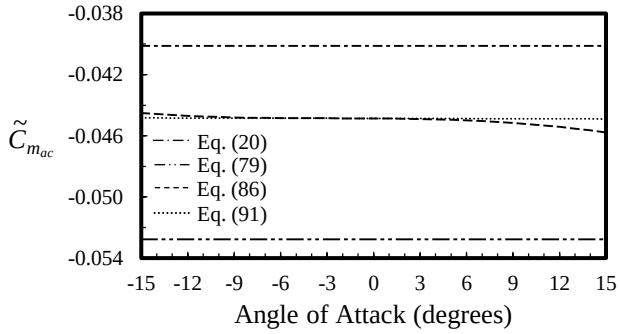

Fig. 10 Pitching moment about the aerodynamic center of the NACA 2412 airfoil as predicted by a traditional method compared to the methods presented in this paper.

First and second derivatives computed from curve fits can be sensitive to the range of data used for the curve fits, especially if the data do not follow the form of the equations to be fit. In order to gain some insight into this sensitivity of the method, the location of the aerodynamic center was estimated using various dataset ranges from the experimental data published by Abbott and von Doenhoff [27] for the NACA 2412 airfoil at a Reynolds number of 3.1 million. Figure 11 shows the estimated aerodynamic center location as computed using the data from four angle-of-attack ranges: −3 to +3 degrees, −6 to +6 degrees, −10 to +10 degrees, and all data below stall onset. Results computed from Eqs. (84) and (85) are shown for angles of attack from −15 degrees to +15 degrees, and results from

the traditional method given in Eq. (7), which are independent of angle of attack, are also included. As can be seen, results from the estimate given in this work as well as the traditional estimate for the aerodynamic center are sensitive to the data ranges used. This is due to variation in the experimental data. The axial variation in results from Eq. (84) is about 0.20%, and that from Eq. (7) is about 0.52%. The vertical variation in results from Eq. (85) is about 14.31%, and that from Eq. (7) is zero due to the fact that the traditional method does not predict any vertical offset of the aerodynamic center for any airfoil. Although the vertical variation from Eq. (85) is noticeably sensitive to variation in the experimental data, it is encouraging to note that the axial location of the aerodynamic center as predicted by Eq. (84) is less sensitive to the variation in the dataset than is the axial location predicted by the traditional method from Eq. (7). These results provide some preliminary insight into the sensitivity of the aerodynamic-center estimates to variation in experimental data. Conclusions drawn from Fig. 11 should not be extrapolated to other data sets or airfoils. A more thorough study of the sensitivities of the methods should be conducted in order to draw any full conclusions as to the robustness of either approach. The purpose of the present work is simply to provide the fundamental aerodynamic theory for more accurately estimating the location of the aerodynamic center.

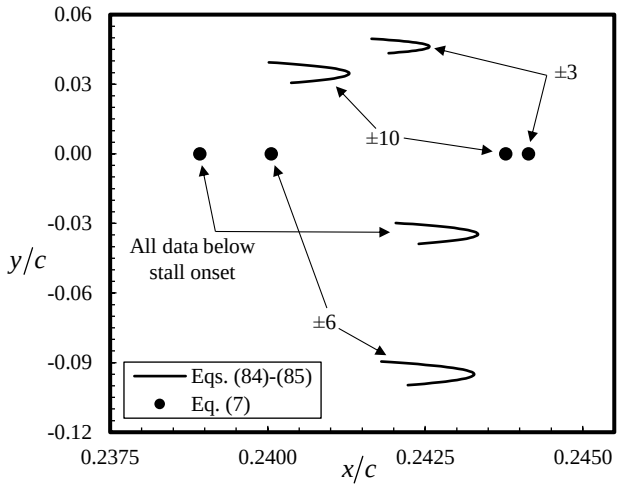

Fig. 11 Aerodynamic center locations for the NACA 2412 airfoil using data in various ranges in angle of attack published by Abbott and von Doenhoff [27].

B. Symmetric Airfoils

For the special case of a symmetric airfoil, the drag is minimized at zero lift, and $\tilde{\tilde{C}}_{D_0,L} = 0$. For this case, Eq. (81) reduces to

$$\tilde{\tilde{C}}_D = \tilde{\tilde{C}}_{D_0} + \tilde{\tilde{C}}_{D_0,L^2}\tilde{\tilde{C}}_L^2 \tag{95}$$

Equation (95) represents a parabola with the vertex at $\tilde{\tilde{C}}_{D_0}$. Because the lift is nearly a linear function of angle of attack, Eq. (95) is very nearly parabolic in angle of attack. Additionally, any parabola can be fit to a cosine function. In this case, it is convenient to express the drag coefficient of a symmetric airfoil as a trigonometric function of angle of attack. We will define an alternate drag parameter $\tilde{\tilde{C}}_{D_s}$ such that the drag given in Eq. (95) can be written in terms of angle of attack as

$$\tilde{\tilde{C}}_D = \tilde{\tilde{C}}_{D_0} + \tilde{\tilde{C}}_{D_s}(1-\cos\alpha) \tag{96}$$

The pitching moment for a symmetric airfoil including viscous effects can be obtained by applying the symmetric relation $\tilde{\tilde{C}}_{m,A} = 0$ from Eq. (60) to the pitching-moment equation given in Eq. (83). This yields

$$\tilde{\tilde{C}}_{m_O} = \tilde{\tilde{C}}_{m0,\alpha}\sin(2\alpha) + \tilde{\tilde{C}}_{m,N}(\tilde{\tilde{C}}_L\cos\alpha + \tilde{\tilde{C}}_D\sin\alpha) \tag{97}$$

Using Eqs. (61) and (96) in Eq. (97) and applying the trigonometric identity $\sin(2\alpha) = 2\sin\alpha\cos\alpha$ gives

$$\tilde{\tilde{C}}_{m_O} = \left[2\tilde{\tilde{C}}_{m0,\alpha} + \tilde{\tilde{C}}_{m,N}\left(\tilde{\tilde{C}}_{L0,\alpha} - \tilde{\tilde{C}}_{D_s} + \frac{\tilde{\tilde{C}}_{D_0} + \tilde{\tilde{C}}_{D_s}}{\cos\alpha}\right)\right]\sin(\alpha)\cos(\alpha) \tag{98}$$

Because the cosine of α is very nearly unity for all angles in the range below stall, the term inside the square brackets in Eq. (98) is very nearly constant for symmetric airfoils below stall, and the pitching moment from Eq. (98) can be closely approximated as

$$\tilde{\tilde{C}}_{m_O} = \tilde{\tilde{C}}_{ms,\alpha}\sin(\alpha)\cos(\alpha) \tag{99}$$

where $\tilde{\tilde{C}}_{ms,\alpha}$ is a constant coefficient. Using Eqs. (61) and (96) in Eqs. (3), (4), and (99), differentiating and applying the result to Eqs. (12)–(13) gives the location of the aerodynamic center for arbitrary symmetric airfoils including viscous effects

$$\frac{x_{ac}}{c} = \tilde{\tilde{C}}_{ms,\alpha} \frac{\kappa_3[2\cos^3(\alpha) - 3\cos(\alpha)] - 2\kappa_4}{\tilde{\tilde{C}}_{D_0}^2 + 3\kappa_3\kappa_4\cos(\alpha) + \kappa_5\tilde{\tilde{C}}_{D_s} + 2\tilde{\tilde{C}}_{L0,\alpha}^2} \tag{100}$$

$$\frac{y_{ac}}{c} = \tilde{\tilde{C}}_{ms,\alpha} \frac{\kappa_3[3 - 2\sin^2(\alpha)]\sin(\alpha)}{\tilde{\tilde{C}}_{D_0}^2 + 3\kappa_3\kappa_4\cos(\alpha) + \kappa_5\tilde{\tilde{C}}_{D_s} + 2\tilde{\tilde{C}}_{L0,\alpha}^2} \tag{101}$$

$$\tilde{\tilde{C}}_{m_{ac}} = -\tilde{\tilde{C}}_{ms,\alpha} \frac{\kappa_3[3\kappa_3\cos(\alpha) + (\tilde{\tilde{C}}_{D_s} + \tilde{\tilde{C}}_{L0,\alpha})\sin^2(\alpha) - 3\tilde{\tilde{C}}_{D_s}]\sin(\alpha)}{\tilde{\tilde{C}}_{D_0}^2 + 3\kappa_3\kappa_4\cos(\alpha) + \kappa_5\tilde{\tilde{C}}_{D_s} + 2\tilde{\tilde{C}}_{L0,\alpha}^2} \tag{102}$$

where

$$\kappa_3 \equiv \tilde{\tilde{C}}_{D_0} + \tilde{\tilde{C}}_{D_s}, \quad \kappa_4 \equiv \tilde{\tilde{C}}_{L0,\alpha} - \tilde{\tilde{C}}_{D_s}, \quad \kappa_5 \equiv 2\tilde{\tilde{C}}_{D_0} + 3\tilde{\tilde{C}}_{D_s} - 4\tilde{\tilde{C}}_{L0,\alpha} \tag{103}$$

Notice that in contrast to Eq. (80), the aerodynamic center of a symmetric airfoil is a function of angle of attack once the effect of viscous drag is included. Additionally, the *y*-coordinate of the aerodynamic center for this case as predicted by Eq. (101) lies on the chord line only when the angle of attack is zero. Hence, even for symmetric airfoils, the aerodynamic center will have a vertical offset that varies with angle of attack.

The coefficients needed in Eqs. (98)–(101) can be computed from a set of numerical or experimental data using a least-squares regression technique. Equation (73) can be used to compute a value for $\dot{\tilde{\tilde{C}}}_{L0,\alpha}$, and Eq. (74) can be used to compute a value for $\dot{\tilde{\tilde{C}}}_{ms,\alpha}$. The coefficients needed for the drag polar in Eq. (96) can be computed from

$$\begin{Bmatrix} \tilde{\tilde{C}}_{D_0} \\ \tilde{\tilde{C}}_{D_s} \end{Bmatrix} = \begin{bmatrix} n & \sum_{i=1}^{n} 1 - \cos\alpha_i \\ \sum_{i=1}^{n} 1 - \cos\alpha_i & \sum_{i=1}^{n} (1 - \cos\alpha_i)^2 \end{bmatrix}^{-1} \begin{Bmatrix} \sum_{i=1}^{n} \tilde{\tilde{C}}_{D_i} \\ \sum_{i=1}^{n} \tilde{\tilde{C}}_{D_i}(1 - \cos\alpha_{i)} \end{Bmatrix} \tag{104}$$

For example, experimental data from Abbott and von Doenhoff [27] were digitized for the NACA 0006, 0009, and 0012 airfoils. These results were fit to Eqs. (61), (96), and (99) using the least-squares regression relations given in Eqs. (73), (74), and (104). The resulting aerodynamic coefficients are shown in Table 3. These coefficients were then used in Eqs. (100) and (101) to obtain the location of the aerodynamic center for each of these airfoils. Results of these computations for the NACA 0006 and 0012 airfoils are included in Fig. 8 for comparison to the results of cambered airfoils. Notice that the vertical position of the aerodynamic center of these symmetric airfoils can vary by 2.5% of the chord over the range $-15 \le \alpha \le 15$.

Table 3. Coefficients for example symmetric NACA airfoils as computed from the vertical least-squares algorithm using data from Abbott and von Doenhoff [27].

NACA	α_{L0}	$\tilde{\tilde{C}}_{L0,\alpha}$	$\tilde{\tilde{C}}_{D_0}$	$\tilde{\tilde{C}}_{D_s}$	$\tilde{\tilde{C}}_{ms,\alpha}$
0006	0.0	6.18958	0.00461	0.78888	-1.55068
0009	0.0	6.10308	0.00551	0.42810	-1.52197
0012	0.0	6.14987	0.00580	0.44154	-1.53301

Note from Fig. 8 that the concavity of the locus of aerodynamic centers for symmetric airfoils is opposite to that of cambered airfoils. The aerodynamic center of symmetric airfoils moves aft with increasing angle-of-attack magnitude, while that for cambered airfoils moves forward. The aerodynamic mechanisms that produce this result are not fully understood at this point. However, it is insightful to compare these results to those for finite wings published by Phillips, Alley, and Niewoehner [3].

In their publication, Phillips et al. computed estimates for the aerodynamic center of a single swept wing with a symmetric airfoil, as well as for a wing-canard combination [3]. The concavity of the aerodynamic centers of symmetric airfoils shown in Fig. 8 match that found from CFD simulations for a single swept wing with a symmetric airfoil [3]. This should not be too surprising since symmetric airfoils and finite wings with symmetric airfoils should have similar symmetric dependence of lift, drag, and pitching moment on angle of attack. Additionally, the concavity of the aerodynamic centers of cambered airfoils shown in Fig. 8 match one estimate of Phillips et al. [3] for a wing-canard configuration with the canard offset vertically from the canard. This, again, should not be too surprising, since the lift, drag, and pitching moment of the canard configuration would produce an asymmetric dependence on angle of attack, similar to that of a cambered airfoil.

The results presented in this work can be used to obtain the location of the aerodynamic center for cambered and symmetric airfoils. Furthermore, because the lift, drag, and pitching moment on a finite wing and/or full aircraft are often assumed to depend on angle of attack in the same form as that of an airfoil, the results of this work have strong implications for estimating the aerodynamic center or neutral point of lifting surfaces in general.

An alternate approach for obtaining the aerodynamic center as a function of angle of attack could be taken by fitting polynomials to experimental data for lift, drag, and pitching moment. These polynomials could then be related to axial and normal forces through Eqs. (3) and (4), and derivatives of these polynomials could be used in Eqs. (12)–(14) to obtain the aerodynamic center and associated pitching moment. Although such an approach can provide accurate numerical solutions, the main benefit to the approach outlined in this paper is that relations between the aerodynamic center and other airfoil properties, such as lift slope or zero-lift angle of attack, can be clearly seen and understood. In contrast, polynomial fits provide little insight into the physics of the problem since the coefficients of the polynomials are somewhat removed from the aerodynamic properties of the airfoil. For airfoils below stall at moderate Reynolds numbers, the nonlinear relations presented in this work should be fairly accurate. However, for more complex cases such as low-Reynolds-number behavior and separation bubbles, employing polynomial fits may be more straight forward in practice.

V. Conclusions

Thin airfoil theory predicts that the aerodynamic center of an airfoil lies at the quarter chord, and this approximation is commonly used today in aircraft design. However, it is widely acknowledged that this is, in general, not correct. Rather, the aerodynamic center lies at the quarter chord only in the limit as the airfoil thickness and camber both approach zero and in the absence of viscosity. Traditional linear methods of predicting the lift and pitching moment coefficients of airfoils as a function of angle of attack neglect trigonometric and aerodynamic nonlinearities associated with the aerodynamics of lifting bodies. Hence, traditional approximations do not accurately predict the location of the aerodynamic center, even below stall.

General nonlinear relations for the ideal lift and pitching moment of arbitrary airfoils as a function of angle of attack below stall have been developed here, which include the trigonometric and aerodynamic nonlinearities of airfoils with arbitrary thickness and camber at arbitrary angles of attack. These general relations are given in Eqs. (42) and (58) for cambered airfoils and in Eqs. (61) and (62) for symmetric airfoils. These relations have been shown to match inviscid airfoil results for arbitrary airfoil geometries to machine precision, whereas the traditional lift and pitching-moment equations based on thin-airfoil theory match the data to only one or two digits. However, **the significance of the general airfoil formulation is not that it more accurately fits experimental data or numerical**

results. Indeed, the accuracy of the traditional equations based on thin airfoil theory is often well within the accuracy of experimental or computational results. **Rather the significance of the general airfoil formulation becomes apparent when second derivatives for lift or pitching moment as a function of angle of attack are needed, which is the case in the estimation of the location of the aerodynamic center.**

Using the general airfoil theory formulation, it has been shown that the aerodynamic center of any arbitrary airfoil in inviscid flow is a single point, independent of angle of attack. For cambered airfoils this position can be computed from Eqs. (77) and (78), and for symmetric airfoils it can be computed from Eq. (80). The corresponding pitching moment about the aerodynamic center is given in Eqs. (79) and (80) respectively. The deviation of this point from the quarter chord can be significant, and example solutions are shown in Fig. 6 for 150 NACA airfoils over a range of thickness and camber.

Estimates for the aerodynamic center based on thin airfoil theory also neglect any effects due to viscosity. It has been shown that, once viscous effects are included, the aerodynamic center is no longer a single point, but is a function of angle of attack. The location of the aerodynamic center including viscous effects can be found for cambered airfoils from Eqs. (84) and (85), and for symmetric airfoils from Eqs. (100) and (101). The associated pitching moment about the aerodynamic center can be obtained from Eqs. (86) and (102) respectively. Because Eqs. (84)–(86) can be cumbersome to implement in practice, a third-order approximation to these solutions is offered in Eqs. (89)–(91). Example solutions for a range of NACA airfoils with varying camber and thickness are shown in Fig. 8, showing that the third-order approximation is in excellent agreement with the exact solutions. Additionally, these results show that the aerodynamic center can deviate from the quarter-chord by more than 3% of the chord. For a wing with an elastic axis located at 35% chord, a deviation in aerodynamic center of 3% relative to the chord is a deviation of 30% relative to the distance between the aerodynamic center and the elastic axis. Therefore, while the difference in the location of the aerodynamic center predicted using thin airfoil theory and the theory presented here is only on the order of a few percent, this can be significant when predicting important aircraft static stability parameters and flutter characteristics.

Acknowledgement

This work was partially funded from the Rocky Mountain Space Grant Consortium under award number NNX15A124H, and by the Office of Naval Research Sea-Based Aviation Program (grant no. N00014-16-1-2074).

References

[1] Hickey, D. P., "Estimation of aerodynamic center and span load distributions of swept wings", *Journal of Aircraft*, Vol. 6, No. 6 (1969), pp. 571-573, doi: 10.2514/3.44110

[2] Phillips, W. F., Hunsaker, D. F., and Niewoehner, R. J., "Estimating the Subsonic Aerodynamic Center and Moment Components for Swept Wings," *Journal of Aircraft*, Vol. 45, No. 3 (2008), pp. 1033-1043, doi: 10.2514/1.33445

[3] Phillips, W. F., Alley, N. R., and Niewoehner, R. J., "Effects of Nonlinearities on Subsonic Aerodynamic Center," *Journal of Aircraft*, Vol. 45, No. 4, July–Aug, 2008, pp. 1244–1255, doi: 10.2514/1.34241

[4] Rodden, W. P., "Methods for Calculating the Subsonic Aerodynamic Center of Finite Wings", *Journal of Aircraft*, Vol. 40, No. 5 (2003), pp. 1003-1003, doi: 10.2514/2.6888

[5] Thompson, M. J., "A Simple Method for Determining the Aerodynamic Center of an Airfoil," *Journal of the Aeronautical Sciences*, Vol. 5, No. 4 (1938), pp. 138-140, doi: 10.2514/8.548

[6] Munk, M. M., "General Theory of Thin Wing Sections," NACA TR-142, Jan. 1922.

[7] Birnbaum, W., "Die tragende Wirbelfläche als Hilfsmittel zur Behandlung des ebenen Problems der Tragflügeltheorie," *Zeitschrift für Angewandte Mathematik und Mechanik*, Vol. 3, No. 4, 1923, pp. 290–297.

[8] Glauert, H., "A Theory of Thin Aerofoils," Aeronautical Research Council, Reports and Memoranda 910, London, Feb. 1924.

[9] Glauert, H., "Thin Aerofoils," *The Elements of Aerofoil and Airscrew Theory*, Cambridge Univ. Press, Cambridge, England, UK, 1926, pp. 87–93.

[10] Abbott, I. H., and von Doenhoff, A. E., "Theory of Thin Wing Sections," *Theory of Wing Sections*, McGraw–Hill, New York, 1949, (republished by Dover, New York, 1959), pp. 64–79.

[11] Anderson, J. D., "Classical Thin Airfoil Theory," *Fundamentals of Aerodynamics, 5th ed.*, McGraw–Hill, New York, 2011, pp. 338–357.

[12] Bertin, J. J., and Cummings, R. M., "Thin-Airfoil Theory," *Aerodynamics for Engineers, 6th ed.*, Prentice–Hall, Upper Saddle River, NJ, 2014, pp. 298–317.

[13] Katz, J., and Plotkin, A., "Small-Disturbance Flow over Two-dimensional Airfoils," *Low-Speed Aerodynamics, 2nd ed.*, Cambridge Univ. Press, Cambridge, England, U.K., 2001, pp. 94–121.

[14] Kuethe, A. M., and Chow, C. Y., "Aerodynamic Characteristics of Airfoils," *Foundations of Aerodynamics: Bases of Aerodynamic Design, 5th ed.*, Wiley, New York, 1998, pp. 136–150.

[15] McCormick, B. W., "Thin Airfoil Theory," *Aerodynamics, Aeronautics, and Flight Mechanics, 2nd ed.*, Wiley, New York, 1995, pp. 73–84.

[16] Phillips, W. F., "Incompressible Flow over Airfoils," *Mechanics of Flight, 2nd ed.*, Wiley, Hoboken, NJ, 2010, pp. 26–39.

[17] Abbott, I. H., and von Doenhoff, A. E., "Theory of Wing Sections of Finite Thickness," *Theory of Wing Sections*, Dover Publications, Inc., New York, 1959, pp. 46–63.

[18] Karamcheti, K., "Problem of the Airfoil," *Principles of Ideal-Fluid Aerodynamics*, Krieger, Malabar, Florida, 1980, pp. 466–491.

[19] Kutta, M. W., "Auftriebskrafte in Stromenenden Flussigkeiten," *Illustrierte Aeronautische Mitteilungen*, Vol. 6, No. 133, 1902.

[20] Joukowski, N. E., "Sur les Tourbillons Adjionts," *Traraux de la Section Physique de la Societe Imperiale des Amis des Sciences Naturales*, Vol. 13, No. 2, 1906.

[21] H. Blasius, "Funktionentheoretische Methoden in der Hydrodynamik," *Zeitschrift für Mathematik und Physik*, Vol. 58, 1910, pp. 90–110.

[22] Hager, W. H., "Blasius: A life in research and education," *Experiments in Fluids*, Vol. 34, 2003, pp. 566–571.

[23] Hunsaker, D. F., Pope, O. D., Hodson, J. D., and Rosqvist, J., "Aerodynamic Centers of Arbitrary Airfoils," 2018 AIAA Aerospace Sciences Meeting, Kissimmee, Florida: American Institute of Aeronautics and Astronautics, 2018, doi:10.2514/6.2018-1276

[24] Phillips, W. F., "The Vortex Panel Method," *Mechanics of* Flight, 2nd ed., Wiley, Hoboken NJ, 2010, pp. 32–39.

[25] Pope, A., "On Airfoil Theory and Experiment," *Journal of the Aeronautical Sciences*, Vol. 15, No. 7, July 1948, pp. 407–410.

[26] Durand, W. F., "The Joukowski Family of Airfoils," *Aerodynamic Theory*, Vol. II, Julius Springer, Berlin, 1935, pp. 68–71.

[27] Abbott, I. H., and von Doenhoff, A. E., "Aerodynamic Characteristics of Wing Sections," *Theory of Wing Sections*, Dover Publications, Inc., New York, 1959, pp. 449–687.

View publication stats